

Monitored long-range interacting systems: spin-wave theory for quantum trajectories

Zejian Li ¹, Anna Delmonte ², Xhek Turkeshi ³, and Rosario Fazio ^{1,4}

¹*The Abdus Salam International Center for Theoretical Physics, Strada Costiera 11, 34151 Trieste, Italy*

²*SISSA, Via Bonomea 265, I-34136 Trieste, Italy*

³*Institut für Theoretische Physik, Universität zu Köln, Zùlpicher Strasse 77, 50937 Köln, Germany*

⁴*Dipartimento di Fisica “E. Pancini”, Università di Napoli “Federico II”, Monte S. Angelo, I-80126 Napoli, Italy*

We introduce a stochastic spin-wave theory tailored to describe quantum trajectories in continuously monitored long-range interacting spin systems. Our method, based on the bosonization of spin-wave excitations on top of a strong collective polarization, enables the efficient simulation of large-scale interacting spins, offering insights into nonlinear features of the dynamics such as entanglement and trajectory correlations. We showcase the versatility of our framework by exploring an entanglement phase transition in a monitored spin system with power-law interactions and dwelling on how our method mitigates the experimental challenges of post-selection in detecting monitored quantum phases.

I. INTRODUCTION

Long-range interacting quantum many-body systems have recently been the focus of intense theoretical and experimental activity [1, 2]. Sufficiently non-local interactions between the elementary constituents of a many-body system lead to exotic non-equilibrium phenomena, with compelling signatures in the properties of quantum correlations and entanglement [3–8], relaxation dynamics [9–11], quantum information scrambling [12–14], and ergodicity-breaking properties [15–17].

Along with their importance in statistical mechanics, long-range quantum systems are central to the rising field of quantum technologies and simulators. Experimental platforms such as trapped ions [18], Bose-Einstein condensates in cavities [19], dipolar [20], polar [21], and Rydberg atoms [22], or driven ultra-cold atomic gases [23] showcase frameworks where the system interactions scale as a power law of the distance. Depending on the experimental platform, the exponent governing the range of the interaction varies and, in some cases, can be tuned, allowing us to explore several different regimes.

The dynamics of long-range systems has been investigated in the opposite limits of unitary and dissipative (Lindbladian) evolutions. In this work, we would like to take a step forward by studying the in-between framework of monitored dynamics. Here, the system evolution is interspersed with quantum measurements, whose outcomes are stochastic. As a result, the system is described by a quantum trajectory conditional to the measurement registry. Averaging the state over the trajectory ensemble recasts a dissipative dynamics, therefore presenting a convenient framework for the study of physical observables, i.e. hermitian operators, in Lindblad dynamics [24–28]. It was more recently realized, in the study of many-body systems, that the quantum trajectory ensemble contains richer information than the mean state, showcased by the several collective phenomena encoded in beyond-average statistical features. The cornerstone examples are monitored quantum phases and measurement-induced phase transitions [29–33], charac-

terized by non-linear functions of the trajectories, such as entanglement probes or trajectory correlation functions. Intensive work gathered insights on the monitored phases in local quantum circuits [34–39], dual-unitary circuits [40–42], monitored non-interacting [43–55] and interacting [56–60] systems, interpolating between strong and weak measurements [61, 62], and presenting a comprehensive understanding in terms of quantum error correction and learning capabilities [63–71].

Experimentally detecting monitored phases, on the other hand, is challenging, and so far limited to few pioneering works on trapped-ions [72] and superconducting platforms [73, 74]. This limitation has a fundamental origin and is known as the *post-selection problem*. Observing beyond average moments of the quantum trajectories requires that one should reproduce the same sequence of measurement outcomes multiple times to collect enough statistics and obtain trajectory expectation values. This task is formidable, as the probability of reproducing the same trajectory is exponentially small in system size and time scale.

The post-selection barrier is in general ineludible for the study of generic many-body monitored systems, and the quest for methods that can mitigate it is an active research line. For instance, the presence of feedback dynamics may be designed to imprint the measurement-induced transition into the density matrix [75, 76], albeit in general leads to separate types of phase transitions [77–84]. A complementary path is pursuable for systems that can be classically simulated. The approach combines the outcome of the quantum evolution and the quantum measurement registry, with the classical post-processing fed by the latter. When the post-processing is efficient and faithful, it allows to elude the post-selection [64, 85–90]. There are special cases in which the system itself is designed to be immune to post-selection. In [91] some of us showed that there is a class of infinite-range spin systems where monitored many-body dynamics can be efficiently realized with a post-selection overhead scaling, at most, as a power of the system size. In Ref. [91], it was argued that this fortunate case was not specific to that model, describing an atomic ensembles driven by a laser field

and in the presence of a collective decay, but it applies to a broad class of monitored systems with an underlying semi-classical dynamics.

A central target of this work is supporting the above claims for sufficiently long-range interacting spin systems. This goal is achieved by

- developing a systematic semi-classical expansion for quantum trajectories that is particularly suited for long-range systems,
- showing that, in this regime, the post-selection barrier is avoidable, paving the way for future experiments. Trapped ions, among others, belong to the systems for which our method and results apply.

Few works have addressed monitored dynamics in long-range interacting systems. Refs. [92, 93] studied Clifford circuits with two-qubit gates entangling distant sites with a probability of decaying as a power-law of their distance. The Floquet dynamics of interacting spin systems with measurements and feedback was considered in a model with entanglement and dissipative phase transitions [94], while monitored long-range free fermions have been studied in Refs. [95, 96]. All these results demonstrate that long-range couplings strongly affect the monitored phases and their transitions: they are relevant in the renormalization group sense.

Here we will show how one can study entanglement dynamics as well as phase transitions in long-range spin systems, by designing a stochastic spin-wave expansion along quantum trajectories. This method will be instrumental in showing how to avoid post-selection in long-range systems. Moreover, the method has a much wider spectrum of applications since the stochastic spin-wave quantum trajectories provide a much more accurate solution to the Lindblad master equation as compared to deterministic spin-wave theories [97].

While the many-body problem renders the exact solution of such systems formidable, long-range interactions typically lead to an underlying semi-classical dynamics that alleviates this difficulty. Consider a system with N fully connected, i.e. infinite-range, spin-1/2 particles with permutation invariance. The entire system then behaves as a single collective spin $S = N/2$. For large N , the collective quantum spin operators, when re-scaled by S , admit vanishingly small ($\sim 1/S$) commutators and hence can be well approximated by a classical continuous spin vector [2]. This is essentially the mean-field approximation, which is exact in the $N \rightarrow \infty$ limit. On top of this classical spin, quantum excitations and fluctuations can then be treated perturbatively. This argument can be extended to long-range models without permutation symmetry, which, by construction, remain close to their infinite-range counterparts, with non-collective excitations decorating the classical spin. These observations lead to a class of approximation methods known as the *spin-wave* theory. Historically, the spin-wave theory was first introduced by Bloch [98] in 1932 for ferro-

magnetic spin systems in equilibrium. An equivalent formulation of the theory was later given by Holstein and Primakoff [99] based on a transformation that now bears their names, that maps spin operators into bosonic ones. To the lowest order of the theory, this can be regarded as approximating the spin system as a set of harmonic oscillators [100], where spin-wave excitations are captured as bosonic quasiparticles. The spin-wave theory has been highly successful in describing equilibrium ground-states in a wide range of magnetic materials, showing good accordance with experimental data [100]. More recently, the spin-wave theory has been generalized to the time-dependent regime [101, 102], capturing non-equilibrium dynamics in closed quantum systems undergoing unitary time evolution governed by a Hamiltonian and in driven-dissipative systems [97] described by a Lindblad master equation. This work enlarges spin-wave theory to encompass generalized measurements, therefore providing the natural framework for the study of monitored Hamiltonian and Lindbladian long-range systems.

The paper is organized as follows. In Section II we set the stage by defining the class of models we are going to examine and the associated average dynamics, the Lindblad equation. Section III is the core of our work as it contains the essence of the stochastic spin-wave approach. In this Section, we explain how it is constructed in the case of a monitored dynamics described by a quantum state diffusion (QSD). The approach can be transposed in a straightforward way to other types of unravelings. We derive the stochastic equations of motions for the spin-waves whose averaged dynamics is described by the Lindblad equation introduced before. The method is then applied in Section IV where we study dissipative phase transitions and entanglement phase transitions in long-range spin systems. In order to test the method we use as a benchmark an infinite-range model where numerically exact calculations can be performed. The agreement is excellent. We then proceed with the generic case where our approach allows us to study large systems, well outside the range of a direct simulation. In Section V we discuss how the post-selection problem can be avoided in long-range spin systems by exploiting quantum-classical cross-correlated observables enabled by our spin-wave framework. Finally, we draw our conclusions in Section VI. Some technical details as well as an extension of our method to spin-boson systems are included in the Appendices.

II. MONITORED LONG-RANGE SPIN SYSTEMS

We consider a system with N spin- s degrees of freedom on a lattice whose sites are labeled by indices i, j , that is subjected to continuous monitoring. For concreteness, we consider the case of weak monitoring where the dynamics is governed by the following stochastic master equation (in units where $\hbar = 1$),

$$d\hat{\rho} = dt\mathcal{L}(\hat{\rho}) + \sum_i \left[dw_i^* \left(\hat{L}_i - \langle \hat{L}_i \rangle \right) \hat{\rho} + dw_i \hat{\rho} \left(\hat{L}_i^\dagger - \langle \hat{L}_i^\dagger \rangle \right) \right], \quad (1)$$

where $\hat{\rho}$ is the density matrix, \mathcal{L} is the Liouvillian superoperator

$$\mathcal{L}(\hat{\rho}) \equiv -i[\hat{H}, \hat{\rho}] + \mathcal{D}(\hat{\rho}), \quad (2)$$

\hat{L}_i are Lindblad operators acting on the i -th spin, and $\langle \hat{L}_i \rangle \equiv \text{Tr}[\hat{\rho}\hat{L}_i]$ denotes the (single-trajectory) expectation value. In Eq. (2), \hat{H} is the Hamiltonian generating the coherent dynamics, whose form we will specify later, and \mathcal{D} denotes the superoperator governing the dissipation, that acts on the density matrix as follows,

$$\mathcal{D}(\hat{\rho}) \equiv \sum_{i,j} f_{ij} \left(\hat{L}_i \hat{\rho} \hat{L}_j^\dagger - \frac{1}{2} \left\{ \hat{L}_j^\dagger \hat{L}_i, \hat{\rho} \right\} \right). \quad (3)$$

The positive semidefinite matrix f_{ij} takes into account spatial correlations among the Lindblad operators \hat{L}_i . In the stochastic master equation (1), dw_i is a complex Wiener process satisfying the relations

$$\overline{dw_i} = 0, \quad (4)$$

$$dw_i^* dw_j = f_{ij} dt, \quad dw_i dw_j = 0,$$

where the $\overline{\bullet}$ notation denotes the ensemble average. Note that in the general case where f_{ij} is nondiagonal, the noises are also spatially correlated.

We consider the dynamics of a pure state $\hat{\rho} = |\psi\rangle\langle\psi|$. Given the purity preservation of the dynamics (1) (cf. Appendix A), the von Neumann entropy

$$S_E \equiv -\text{Tr} \left[\hat{\rho}_{\frac{N}{2}} \log \hat{\rho}_{\frac{N}{2}} \right] \quad (5)$$

is a good quantifier of entanglement [103]. Here, $\hat{\rho}_{\frac{N}{2}} \equiv \text{Tr}_{\{1, \dots, \lfloor N/2 \rfloor\}} [|\psi\rangle\langle\psi|]$ denotes the reduced density matrix of half of the system (in a bipartition where one subsystem contains spins indexed from 1 to $\lfloor N/2 \rfloor$).

Using Eqs. (1) and (4), one verifies that the trajectory-average state (which we also denote by $\hat{\rho}$ when there is no confusion with the single-trajectory state) evolves deterministically according to the Lindblad master equation

$$\frac{d}{dt} \hat{\rho} = \mathcal{L}(\hat{\rho}). \quad (6)$$

As shown in the Appendix A, Eq. (1) is an unraveling of the master equation (6) and describes the quantum state diffusion process subjected to a heterodyne-detection monitoring scheme [25, 104].

A. Power-law spin model

While the formulation of our spin-wave method will not depend on the particular form of the model, we generally

require \hat{H} and \mathcal{D} to be long-range in order for the method to yield an accurate approximation to the exact solution. For concreteness, we study a prototypical driven-dissipative spin model with spatially extended interaction whose strength decays as a power-law according to the distance. The model is defined on a one-dimensional periodic chain with Hamiltonian

$$\hat{H} = \omega \hat{S}^x + \frac{2sJ}{\mathcal{N}} \sum_{i,j} \frac{\hat{\sigma}_i^z \hat{\sigma}_j^z}{d(i,j)^\alpha}, \quad (7)$$

where ω is the amplitude of a collective drive and J is the interaction strength. The factor $2s$ ensures that the mean-field theory (see Appendix B) is s -independent, which can be ignored for spin-half ($s = 1/2$) systems. Here, we denote total spin operators with the capital \hat{S}^μ , $\mu \in \{x, y, z\}$ without the site index subscript

$$\hat{S}^\mu \equiv \sum_i \hat{s}_i^\mu, \quad (8)$$

while the total spin number is denoted by

$$S \equiv \mathcal{N}s. \quad (9)$$

The lower-case notation \hat{s}_i^μ refers to the spin operator of the i -th site, which satisfies the standard $\mathfrak{su}(2)$ algebra

$$[\hat{s}_i^\mu, \hat{s}_j^\nu] = i\delta_{ij} \epsilon^{\mu\nu\gamma} \hat{s}_i^\gamma. \quad (10)$$

We denote the normalized spin operators with

$$\hat{\sigma}_i^\mu \equiv \hat{s}_i^\mu / s, \quad (11)$$

which reduce to the standard Pauli matrices in the case of spin-half. The distance on the periodic chain is

$$d(i, j) \equiv \min(|i - j|, N - |i - j|), \quad (12)$$

and in the case of $i = j$ we adopt the convention of $d(i, i) = \infty$ such that there is no on-site self-interaction for finite α . The Kac normalization [105]

$$\mathcal{N} \equiv \frac{1}{N} \sum_{i,j} \frac{1}{d(i, j)^\alpha}, \quad (13)$$

ensures a well-defined thermodynamic limit for the interaction Hamiltonian. The power α determines the range of the interaction. In particular, the case of $\alpha = 0$ describes an infinite-range model with permutation invariance, and the opposite limit $\alpha \rightarrow \infty$ corresponds to an Ising model with nearest-neighbor interaction. The long-range regime corresponds to the case where $0 < \alpha < 1$.

In addition to the unitary dynamics governed by the Hamiltonian, we subject the spin chain to a collective (infinite-range) decay, a case of experimental relevance [23, 106], resulting in the following Lindblad master equation,

$$\frac{d\hat{\rho}}{dt} = -i[\hat{H}, \hat{\rho}] + \frac{\kappa}{S} \left(\hat{S}^- \hat{\rho} \hat{S}^+ - \frac{1}{2} \left\{ \hat{S}^+ \hat{S}^-, \hat{\rho} \right\} \right), \quad (14)$$

with S serving the role of Kac normalization for the dissipator, κ is the dissipation strength, and $\hat{S}^\pm \equiv \hat{S}^x \pm i\hat{S}^y$ are the collective spin raising and lowering operators. Note that this collective dissipator corresponds to the choice of $f_{ij} = \kappa/S = \text{const}$ and $\hat{L}_i = \hat{s}_i^- = \hat{s}_i^x - i\hat{s}_i^y$ in terms of our generic notation in Eq. (3).

In the mean-field approximation, the system is predicted to exhibit a continuous phase transition from a stationary phase to a time-crystal one. In the stationary phase, the mean-field steady-state z -magnetization is

$$\frac{\langle \hat{S}^z \rangle_{\text{MF}}}{S} = -\sqrt{1 - \frac{\omega^2}{16J^2 + \kappa^2}}, \quad (15)$$

cf. Appendix B. This stationary phase terminates at a critical point $\omega_{\text{MF}}^{(c)} = \sqrt{16J^2 + \kappa^2}$, beyond which the z -magnetization admits only permanently oscillating solutions with zero mean when averaged over long times.

This model has been previously studied in [91] to demonstrate an entanglement phase transition in the unraveled dynamics in the case of $J = 0$, which is an infinite-range collective model. In this regime, the system displays an entanglement phase transition coinciding with the dissipative phase transition from the stationary phase to the time-crystal phase. This transition also features a fast saturation of the entanglement entropy, making its experimental detection free from the exponential post-selection overhead. It was also hypothesized in [91] that the above results should hold in the presence of sufficiently long-range interactions, which was supported by numerical evidence for the case $J \neq 0$ and $\alpha \neq 0$ for up to 10 spin-1/2 sites since the exact simulation requires the full 2^N -dimensional Hilbert space and is not feasible for thermodynamically large N . In the following section, we develop the theory of spin-wave quantum trajectories, allowing us to overcome the above limitations and tackle the problem in the thermodynamic limit. Our results are presented in Sec. IV.

III. SPIN-WAVE THEORY ALONG QUANTUM TRAJECTORIES

In this section, we formulate the theory of non-equilibrium spin-wave quantum trajectories (SWQT) and derive the equations of motion for spin systems under continuous monitoring. This formalism serves as a semi-classical method for solving quantum trajectories of generic out-of-equilibrium dissipative spin systems with sufficiently long-range interactions whose average dynamics can be described by a Lindblad master equation. In previous studies [97], the non-equilibrium spin-wave theory has been generalized to dissipative spin systems on the level of the averaged state, i.e. the density matrix evolving deterministically under the master equation, cf. Eq. (6). This technique has been proven successful in studying dissipative dynamics of large N over extended time spans. Our method, on the other hand,

resolves the dynamics on the level of *single quantum trajectories*, corresponding to the unravelling (1) of the master equation, enabling us to probe non-linear quantum-trajectory correlations, encoded in the entanglement and other non-linear functions of the state [107].

The central assumption is that the system admits a strong collective spin polarization, on top of which spin-wave excitations are bosonized via a truncated Holstein-Primakoff expansion. The bosonic modes are then approximated with a Gaussian ansatz [108, 109] parametrized by first and second moments. We remark that, since our assumption is formulated at the level of single trajectories and not at the level of average dynamics, our variational ansatz allows us to reach a larger class of density matrices compared to previous methods [109]. Indeed, the mixture of Gaussian states, such as those describing single trajectories, is a non-Gaussian state in general, hence encodes non-trivial correlations between the spin-waves. This fact has a fundamental operational consequence: spin-wave quantum trajectories provide more accurate representations of the purely Lindblad dynamics [109], making the SWQT compelling also for the study of the dissipative dynamics of hermitian operators.

The main challenge in the generalization of spin-wave theory to quantum trajectories comes from the fact that the state no longer follows a smooth deterministic evolution, as the density matrix does, but rather evolves stochastically, whereas the bosonization of spin-wave excitations has to be performed in the instantaneous frame aligned with the collective spin polarization in order to yield a valid approximation. In the case of interest, the evolution is continuous but nowhere differentiable. Therefore, a naive rotating frame cannot be directly applied. Therefore, we base our approach on the Euler-Maruyama [110] method to determine the coupled stochastic evolution of the state and of the frame in a self-consistent way.

The rest of the section is organized as follows. In Sec. III A, we introduce the major approximations made in the spin-wave theory, namely the truncated Holstein-Primakoff expansion and the Gaussian approximation. Then, We derive the equations of motion in Sec. III B.

A. Spin-wave approximation

To keep the discussion self-consistent, we introduce in this subsection the key approximations made in our spin-wave theory, namely the truncated Holstein-Primakoff transformation and the Gaussian approximation. These approximations will bosonize the spin fluctuations on top of a moving vacuum defined by the collective polarization of all spins, and then approximate the bosonic fluctuations up to the Gaussian, i.e. quadratic, level.

To prepare for this discussion, let us now consider a generic rotated reference frame $O\tilde{x}\tilde{y}\tilde{z}$ defined by the unitary transformation parametrized by angles θ and ϕ [see

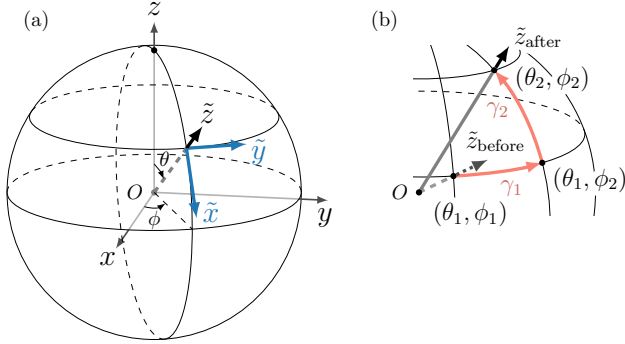


Figure 1. (a) Sketch of the reference frames considered in our method. $Oxyz$ is the lab frame and $O\tilde{x}\tilde{y}\tilde{z}$ represents the instantaneous frame where \tilde{z} aligns with the collective mode polarization. For illustration purposes, the axes \tilde{x} and \tilde{y} are moved from the origin to the surface of the sphere for clarity. (b) Sketch of the re-alignment of the reference frame where the frame angles (θ, ϕ) are updated to match the collective spin direction after its evolution in an infinitesimal time step. The curved arrows represent the paths γ_1 and γ_2 as defined in Eq. (36) for evaluating the integral of Eq. (35). The dashed (solid) straight arrow represents the \tilde{z} axis before (after) the re-alignment step.

Fig. 1 (a) for an illustration of the rotated frame]

$$\hat{U}(\theta, \phi) = e^{-i\phi\hat{S}^z} e^{-i\theta\hat{S}^y}. \quad (16)$$

The spin operators associated with the rotated frame are given by

$$\hat{s}_i^{\tilde{\alpha}} = \hat{U}(\theta, \phi)\hat{s}_i^{\alpha}\hat{U}^{\dagger}(\theta, \phi) = \sum_{\beta} G_{\tilde{\alpha}\beta}\hat{s}_i^{\beta}, \quad (17)$$

where $G_{\tilde{\alpha}\beta} \equiv \mathbf{e}_{\tilde{\alpha}} \cdot \mathbf{e}_{\beta}$ is the 3×3 matrix representing the spatial rotation

$$G = \begin{pmatrix} \cos\theta \cos\phi & \cos\theta \sin\phi & -\sin\theta \\ -\sin\phi & \cos\phi & 0 \\ \sin\theta \cos\phi & \sin\theta \sin\phi & \cos\theta \end{pmatrix}. \quad (18)$$

Here, the rows of G are the rotated unit vectors $\mathbf{e}_{\tilde{x}}$, $\mathbf{e}_{\tilde{y}}$ and $\mathbf{e}_{\tilde{z}}$ (assuming $\{\mathbf{e}_{\alpha}\}_{\alpha}$ to be the canonical basis for the lab frame). The inverse transformation

$$\hat{s}_i^{\beta} = \sum_{\tilde{\alpha}} G_{\tilde{\alpha}\beta}\hat{s}_i^{\tilde{\alpha}}, \quad (19)$$

allows us to express all the operators in the rotated frame. We now choose the frame angles (θ, ϕ) such that the rotated \tilde{z} aligns with the direction of the collective spin

$$\langle \hat{S}^{\tilde{x}} \rangle = \langle \hat{S}^{\tilde{y}} \rangle = 0. \quad (20)$$

This allows us to approximate the spin operators with a Holstein-Primakoff transformation truncated to the low-

est order

$$\begin{aligned} \hat{s}_i^{\tilde{z}} &= s - \hat{b}_i^{\dagger}\hat{b}_i, \\ \hat{s}_i^{\tilde{x}} &\simeq \sqrt{\frac{s}{2}}(\hat{b}_i^{\dagger} + \hat{b}_i), \\ \hat{s}_i^{\tilde{y}} &\simeq i\sqrt{\frac{s}{2}}(\hat{b}_i^{\dagger} - \hat{b}_i), \end{aligned} \quad (21)$$

where \hat{b}_i 's are bosonic operators with standard bosonic commutation relations $[\hat{b}_i, \hat{b}_j^{\dagger}] = \delta_{ij}$. This transformation effectively approximates the Bloch sphere with the tangent plane at the north pole of the rotated frame [2], which is why we need to align \tilde{z} with the collective spin direction. This approximation becomes exact only when $\langle \hat{b}_i^{\dagger}\hat{b}_i \rangle = 0$, i.e., when the system is in a spin coherent state. Thus, the density of bosonic excitations

$$\epsilon \equiv \frac{1}{N_s} \sum_i \langle \hat{b}_i^{\dagger}\hat{b}_i \rangle, \quad (22)$$

serves as a natural control parameter for the approximation. In the regime of $\epsilon \ll 1$, the bosonization in Eq. (21) faithfully captures the spin dynamics without higher-order corrections [97]. The bosonic modes \hat{b}_i represent spin-wave excitations on top of the collective polarization. We will therefore refer to the control parameter ϵ as the *spin-wave density*.

Let us now make our second approximation, where we assume the state of the bosonic modes to be Gaussian along each trajectory. This allows us to uniquely specify the state of the entire system with the following variational parameters:

$$\theta, \phi, \beta_i \equiv \langle \hat{b}_i \rangle, u_{ij} \equiv \langle \hat{\delta}_i \hat{\delta}_j \rangle, v_{ij} \equiv \langle \hat{\delta}_i^{\dagger} \hat{\delta}_j \rangle, \quad (23)$$

where $\hat{\delta}_i \equiv \hat{b}_i - \beta_i$. Therefore, this method requires only $\mathcal{O}(N^2)$ parameters to represent the state in the most general case, which is exponentially efficient as compared to the dimension of the full Hilbert space 2^N . The complexity can be further reduced if additional symmetry is present in the dynamics. For example, the power-law spin model introduced in Sec. II A preserves translational invariance on the level of single trajectories. Therefore, the covariances u_{ij} and v_{ij} will depend only on the distance between sites i and j , which reduces the number of parameters to $\mathcal{O}(N)$.

The Gaussian approximation, as a variational ansatz, allows us to calculate any physical quantity of the state within the approximation. In particular, the entanglement between spins can be readily obtained using the covariance formalism of Gaussian states [111], see Appendix C for details.

B. Equations of motion

In order to derive the unraveled dynamics under the spin-wave approximation introduced in the previous subsection, we should provide the rules for updating the

variational parameters of the state, θ , ϕ , β_i , u_{ij} and v_{ij} according to the stochastic unraveling defined in Eq. (1). Our algorithm is based on the Euler–Maruyama method [110], where time is discretized into small steps. Initializing the parameters at $t = 0$ such that the rotated frame parametrized by (θ, ϕ) has its \tilde{z} axis aligned with the collective spin (which implies $\sum_i \beta_i = 0$), we proceed stroboscopically by repeating the two following steps until the desired time t is reached:

1. Calculate the infinitesimal increments for the Gaussian parameters $\delta\beta_i$, δu_{ij} and δv_{ij} using Eq. (1), and update these quantities with the increments. Note that the frame angles (θ, ϕ) are kept constant within this step, which implies that the \tilde{z} axis no longer aligns with the collective spin after the update as $\sum_i \delta\beta_i \neq 0$ in general.
2. Update frame angles (θ, ϕ) such that $\sum_i \beta_i = 0$ in the new rotated frame [see Fig. 1 (b) for a schematic representation of this step]. This can be achieved self-consistently by considering the evolution of the bosonic mode \hat{b}_i generated by the (passive) rotation of the frame alone. Then update the Gaussian parameters β_i , u_{ij} and v_{ij} accordingly (due to the rotation of the frame). Finally, increase the time by δt and start a new iteration.

The re-alignment of the reference frame $O\tilde{x}\tilde{y}\tilde{z}$ in step 2 above is essential to the validity of the truncated Holstein–Primakoff bosonization approximation (which is only sound for small deviations of the spin from the north pole of the Bloch sphere). This will allow the accurate representation of the dynamics over an extended time window significantly beyond the restrictions of a conventional spin-wave theory bosonizing in a static reference frame.

We detail below the key ingredients for performing the two steps sketched above.

1. Infinitesimal increments

The stochastic master equation (1) presented in Sec. II determines the time evolution of the expectation value of operators. For a time-independent operator \hat{O} , the expectation $\langle \hat{O} \rangle = \text{Tr}[\hat{\rho}\hat{O}]$ evolves as follows,

$$\begin{aligned} d\langle \hat{O} \rangle &= dt \langle \mathcal{L}^\dagger(\hat{O}) \rangle + \sum_i \left[dw_i^* \left(\langle \hat{O}\hat{L}_i \rangle - \langle \hat{O} \rangle \langle \hat{L}_i \rangle \right) \right. \\ &\quad \left. + dw_i \left(\langle \hat{L}_i^\dagger \hat{O} \rangle - \langle \hat{L}_i^\dagger \rangle \langle \hat{O} \rangle \right) \right], \end{aligned} \quad (24)$$

where \mathcal{L}^\dagger is the adjoint Liouvillian:

$$\mathcal{L}^\dagger(\hat{O}) \equiv i[\hat{H}, \hat{O}] + \sum_{i,j} f_{ij} \left(\hat{L}_j^\dagger \hat{O} \hat{L}_i - \frac{1}{2} \{ \hat{L}_j^\dagger \hat{L}_i, \hat{O} \} \right). \quad (25)$$

The infinitesimal increments for the expectation of the time-independent operator \hat{b}_i can be therefore obtained by setting $\hat{O} = \hat{b}_i$ in Eq. (24):

$$\begin{aligned} d\beta_i &= d\langle \hat{b}_i \rangle \\ &= \text{idt} \langle [\hat{H}, \hat{b}_i] \rangle \\ &\quad + dt \sum_{j,l} f_{jl} \left\langle \hat{L}_l^\dagger \hat{b}_i \hat{L}_j - \frac{1}{2} \{ \hat{L}_l^\dagger \hat{L}_j, \hat{b}_i \} \right\rangle \\ &\quad + \sum_l \left(dw_l^* \langle \hat{\delta}_i \hat{L}_l \rangle + dw_l \langle \hat{L}_l^\dagger \hat{\delta}_i \rangle \right). \end{aligned} \quad (26)$$

For the two-point covariance u_{ij} , which is the expectation of the time-dependent observable $\hat{\delta}_i \hat{\delta}_j$, their increments can be obtained using the Ito differentiation rule:

$$\begin{aligned} du_{ij} &= d\langle \hat{\delta}_i \hat{\delta}_j \rangle \\ &= \text{idt} \langle [\hat{H}, \hat{\delta}_i \hat{\delta}_j] \rangle \\ &\quad + dt \sum_{l,m} f_{lm} \left\langle \hat{L}_m^\dagger \hat{\delta}_i \hat{\delta}_j \hat{L}_l - \frac{1}{2} \{ \hat{L}_m^\dagger \hat{L}_l, \hat{\delta}_i \hat{\delta}_j \} \right\rangle \\ &\quad + \sum_l \left[dw_l^* \left\langle (\hat{\delta}_i \hat{\delta}_j - u_{ij}) \hat{L}_l \right\rangle \right. \\ &\quad \left. + dw_l \left\langle \hat{L}_l^\dagger (\hat{\delta}_i \hat{\delta}_j - u_{ij}) \right\rangle \right] \\ &\quad - dt \sum_{l,m} \left(f_{lm} \langle \hat{\delta}_i \hat{L}_l \rangle \langle \hat{L}_m^\dagger \hat{\delta}_j \rangle + f_{ml} \langle \hat{\delta}_j \hat{L}_m \rangle \langle \hat{L}_l^\dagger \hat{\delta}_i \rangle \right). \end{aligned} \quad (27)$$

where the last term proportional to dt comes from the time-dependence of $\hat{\delta}_i \hat{\delta}_j$. Similarly, we have for v_{ij} ,

$$\begin{aligned} dv_{ij} &= d\langle \hat{\delta}_i^\dagger \hat{\delta}_j \rangle \\ &= \text{idt} \langle [\hat{H}, \hat{\delta}_i^\dagger \hat{\delta}_j] \rangle \\ &\quad + dt \sum_{l,m} f_{lm} \left\langle \hat{L}_m^\dagger \hat{\delta}_i^\dagger \hat{\delta}_j \hat{L}_l - \frac{1}{2} \{ \hat{L}_m^\dagger \hat{L}_l, \hat{\delta}_i^\dagger \hat{\delta}_j \} \right\rangle \\ &\quad + \sum_l \left[dw_l^* \left\langle (\hat{\delta}_i^\dagger \hat{\delta}_j - v_{ij}) \hat{L}_l \right\rangle \right. \\ &\quad \left. + dw_l \left\langle \hat{L}_l^\dagger (\hat{\delta}_i^\dagger \hat{\delta}_j - v_{ij}) \right\rangle \right] \\ &\quad - dt \sum_{l,m} \left(f_{lm} \langle \hat{\delta}_i^\dagger \hat{L}_l \rangle \langle \hat{L}_m^\dagger \hat{\delta}_j \rangle + f_{ml} \langle \hat{\delta}_j \hat{L}_m \rangle \langle \hat{L}_l^\dagger \hat{\delta}_i^\dagger \rangle \right). \end{aligned} \quad (28)$$

In the equations above, the Hamiltonian \hat{H} and the dissipation operators \hat{L}_i should be expressed in terms of the bosonic operators \hat{b}_i using the substitution rules defined in Eqs. (19) and (21). The Gaussian approximation then allows evaluating the expectation value of every term beyond quadratic order in \hat{b}_i in terms of one- and two-point correlators, i.e. β_i , u_{ij} and v_{ij} , thanks to the Wick theorem. The increments $\delta\beta_i$, δu_{ij} , and δv_{ij} are then calculated using the discretized versions of the equations above. This can be achieved with the substitution

$dt \rightarrow \delta t$ for a sufficiently small time step δt . The noise is approximated with $dw_i \rightarrow \delta w_i = \sqrt{\delta t}(X_i + iY_i)$, where the pair of random vectors (\mathbf{X}, \mathbf{Y}) at every time step is drawn from a multivariate real Gaussian distribution with zero mean and the following covariance matrix [112],

$$\mathbf{K} = \begin{pmatrix} \mathbf{K}^{\mathbf{X}\mathbf{X}} & \mathbf{K}^{\mathbf{X}\mathbf{Y}} \\ \mathbf{K}^{\mathbf{Y}\mathbf{X}} & \mathbf{K}^{\mathbf{Y}\mathbf{Y}} \end{pmatrix} \quad (29)$$

with matrix elements

$$\begin{aligned} (\mathbf{K}^{\mathbf{X}\mathbf{X}})_{ij} &= (\mathbf{K}^{\mathbf{Y}\mathbf{Y}})_{ij} = \frac{1}{2} \text{Re } f_{ij}, \\ (\mathbf{K}^{\mathbf{X}\mathbf{Y}})_{ij} &= -(\mathbf{K}^{\mathbf{Y}\mathbf{X}})_{ij} = \frac{1}{2} \text{Im } f_{ij}. \end{aligned} \quad (30)$$

We complete this step by updating the Gaussian parameters with the increments obtained following the prescription described above:

$$\begin{aligned} \beta_i &\leftarrow \beta_i + \delta\beta_i, \\ u_{ij} &\leftarrow u_{ij} + \delta u_{ij}, \\ v_{ij} &\leftarrow v_{ij} + \delta v_{ij}. \end{aligned} \quad (31)$$

As a result of the truncated Holstein-Primakoff expansion at the lowest order, the increments include terms up to first order in $1/S$, which account for finite-size effects in the dynamics as a correction to the mean-field (zeroth order) theory.

2. Re-alignment of the frame

After the infinitesimal evolution of the state, let us update the reference frame such that the \tilde{z} axis aligns with the updated direction of the collective spin. This condition is equivalent to requiring the following quantity to be zero,

$$\underline{\beta} \equiv \frac{1}{N} \sum_{i=1}^N \beta_i, \quad (32)$$

as a direct implication of Eqs. (20) and (21). This can be achieved by moving the frame smoothly along a path $\theta(\tau), \phi(\tau)$ parametrized by some parameter τ . The unitary transformation defined in Eq. (16) therefore becomes τ -dependent,

$$\hat{U}(\tau) = \hat{U}(\theta(\tau), \phi(\tau)). \quad (33)$$

The rotation of the frame induces some apparent (fictitious) dynamics on the state, whose generator takes the form of an ‘‘inertial Hamiltonian’’:

$$\begin{aligned} \hat{H}_{\text{RF}} &= -i \frac{d\hat{U}}{d\tau} \hat{U}^\dagger \\ &= \sin\theta \frac{d\phi}{d\tau} \hat{S}^{\tilde{x}} - \frac{d\theta}{d\tau} \hat{S}^{\tilde{y}} - \cos\theta \frac{d\phi}{d\tau} \hat{S}^{\tilde{z}}. \end{aligned} \quad (34)$$

We then use the bosonization rules in Eq. (21) to substitute the spin operators with bosonic ones to express

\hat{H}_{RF} in terms of \hat{b}_i . To find the amount of rotation of the frame to achieve $\underline{\beta} = 0$, let us consider the apparent evolution of the operator \hat{b}_i along the moving frame:

$$\begin{aligned} \frac{d\hat{b}_i}{d\tau} &= i \left[\hat{H}_{\text{RF}}, \hat{b}_i \right] \\ &= -i \sqrt{\frac{s}{2}} \sin\theta \frac{d\phi}{d\tau} - \sqrt{\frac{s}{2}} \frac{d\theta}{d\tau} - i \cos\theta \frac{d\phi}{d\tau} \hat{b}_i. \end{aligned} \quad (35)$$

This equation can be integrated analytically by considering the path on the Bloch sphere from (θ_1, ϕ_1) to (θ_2, ϕ_2) following the two segments [as illustrated in 1 (b)]:

$$\begin{aligned} \gamma_1 : \theta(\tau) &= \theta_1, \phi(\tau=0) = \phi_1, \phi(\tau=1) = \phi_2; \\ \gamma_2 : \phi(\tau) &= \phi_2, \theta(\tau=1) = \theta_1, \theta(\tau=2) = \theta_2. \end{aligned} \quad (36)$$

In the first segment γ_1 , we are following a latitude line of constant θ , and the evolution equation simplifies to be a separable first-order differential equation of $\hat{b}_i(\phi)_{\theta=\theta_1}$:

$$d\hat{b}_i(\phi) = i \sqrt{\frac{s}{2}} \sin\theta_1 d\phi - i \cos\theta_1 \hat{b}_i d\phi, \quad (37)$$

which can be solved as

$$\begin{aligned} \hat{b}_i(\theta_1, \phi_2) &= \left[\sqrt{\frac{s}{2}} \tan\theta_1 + \hat{b}_i(\theta_1, \phi_1) \right] e^{-i\Delta\phi \cos\theta_1} \\ &\quad - \sqrt{\frac{s}{2}} \tan\theta_1, \end{aligned} \quad (38)$$

where $\Delta\phi \equiv \phi_2 - \phi_1$. The evolution along the second segment, following a longitude line of constant ϕ , is simply

$$d\hat{b}_i(\theta) = -\sqrt{\frac{s}{2}} d\theta, \quad (39)$$

which gives

$$\begin{aligned} \hat{b}_i(\theta_2, \phi_2) &= \hat{b}_i(\theta_1, \phi_2) - \sqrt{\frac{s}{2}} \Delta\theta \\ &= \left[\sqrt{\frac{s}{2}} \tan\theta_1 + \hat{b}_i(\theta_1, \phi_1) \right] e^{-i\Delta\phi \cos\theta_1} \\ &\quad - \sqrt{\frac{s}{2}} \tan\theta_1 - \sqrt{\frac{s}{2}} \Delta\theta, \end{aligned} \quad (40)$$

where $\Delta\theta \equiv \theta_2 - \theta_1$. This equation immediately implies the evolution of $\underline{\beta}$, upon taking the expectation of both sides,

$$\begin{aligned} \underline{\beta}(\theta_2, \phi_2) &= \left[\sqrt{\frac{s}{2}} \tan\theta_1 + \underline{\beta}(\theta_1, \phi_1) \right] e^{-i\Delta\phi \cos\theta_1} \\ &\quad - \sqrt{\frac{s}{2}} \tan\theta_1 - \sqrt{\frac{s}{2}} \Delta\theta. \end{aligned} \quad (41)$$

As our objective is to find the amount of rotations $\Delta\theta$ and $\Delta\phi$ starting from $\theta_1 = \theta$ and $\phi_1 = \phi$ such that $\underline{\beta}(\theta + \Delta\theta, \phi + \Delta\phi) = 0$, we simply set the right-hand side

of the equation above to zero, giving our final expressions for the angle increments:

$$\begin{aligned}\Delta\phi &= \frac{1}{\cos\theta} \arctan\left\{\frac{\text{Im}\underline{\beta}}{\sqrt{\frac{s}{2}}\tan\theta + \text{Re}\underline{\beta}}\right\} \\ \Delta\theta &= \left(\tan\theta + \sqrt{\frac{2}{s}}\text{Re}\underline{\beta}\right)\cos(\Delta\phi\cos\theta) \\ &+ \sqrt{\frac{2}{s}}\text{Im}\underline{\beta}\sin(\Delta\phi\cos\theta) - \tan\theta.\end{aligned}\quad (42)$$

Note that these increments are not necessarily infinitesimal due to the coordinate singularities near the poles of the Bloch sphere, where the angle ϕ may change drastically even for physically small movements of the frame. With the angular increments in hand, we are now ready to update the remaining parameters, namely the one- and two-point correlators for the bosonic Gaussian state. The first moments β_i can be updated directly using Eq. (40) with the operator \hat{b}_i replaced by its expectation value β_i . This equation also implies the evolution of the fluctuation operators $\hat{\delta}_i = \hat{b}_i - \beta_i$, which is simply

$$\hat{\delta}_i(\theta_2, \phi_2) = \hat{\delta}_i(\theta_1, \phi_1)e^{-i\Delta\phi\cos\theta_1}.\quad (43)$$

We obtain, therefore,

$$\begin{aligned}u_{ij}(\theta_2, \phi_2) &= u_{ij}(\theta_1, \phi_1)e^{-2i\Delta\phi\cos\theta_1}, \\ v_{ij}(\theta_2, \phi_2) &= v_{ij}(\theta_1, \phi_1).\end{aligned}\quad (44)$$

With this, we complete the full update step, summarized as follows:

$$\begin{aligned}\theta &\leftarrow \theta + \Delta\theta, \\ \phi &\leftarrow \phi + \Delta\phi, \\ \beta_i &\leftarrow \left[\sqrt{\frac{s}{2}}\tan\theta + \beta_i\right]e^{-i\Delta\phi\cos\theta} \\ &\quad - \sqrt{\frac{s}{2}}\tan\theta - \sqrt{\frac{s}{2}}\Delta\theta, \\ u_{ij} &\leftarrow u_{ij}e^{-2i\Delta\phi\cos\theta}, \\ v_{ij} &\leftarrow v_{ij}.\end{aligned}\quad (45)$$

Finally, we increase the (physical) time t to the next step $t \leftarrow t + \delta t$ and we are ready for a new iteration.

Let us briefly recap the operations performed in each time step of the algorithm. We first update the Gaussian parameters β_i , u_{ij} and v_{ij} according to Eq. (31) using the increments computed from Eqs. (26)-(28). We then perform the re-alignment step which updates the variational parameters according to Eq. (45) using the angular increments $\Delta\theta$ and $\Delta\phi$ given by Eq. (42), completing the full iteration.

Lastly, note that our method presented above is fully generic, as it suffices to systematically apply the bosonization and the Gaussian approximation to obtain the equations of motion. Therefore, it can be straightforwardly extended to other types of systems beyond those

we considered. An example of its generalization to spin-boson systems is presented in Appendix D together with some illustrative numerical results.

IV. RESULTS

In this section, we apply the presented theory of spin-wave quantum trajectories to study the power-law interacting spin model introduced in Sec. II A. We focus on $s = 1/2$ and fix the interaction strength at $J = 0.1\kappa$ for the rest of the section.

A. Infinite-range case: $\alpha = 0$

We now test the quality of the approximation by evaluating both linear (e.g., observables) and non-linear (e.g., entanglement entropy) functions of the state. In order to benchmark the method, we first revisit the known case of $\alpha = 0$, where the $z - z$ interaction is all-to-all with no spatial resolution. In this regime, the system can be effectively represented as a single spin $S = N/2$, and the Hamiltonian (7) becomes

$$\hat{H} = \omega\hat{S}^x + \frac{2J}{S}(\hat{S}^z)^2.\quad (46)$$

This allows us to benchmark the spin-wave method against the exact simulation of the dynamics of the collective mode in the Dicke basis. Note that the computational complexity of our spin-wave method also significantly reduces in this case since it suffices to apply the formalism in Sec. III to an effective single-body problem with spin number S . This boils down to calculating three increments at each step: $\delta\beta$, δu , and δv ; the re-alignment step then gives the angular increments $\Delta\theta$ and $\Delta\phi$, resets β to zero and applies a phase factor to u . The computation cost is therefore constant for the spin-wave method, which is still significantly more efficient than the exact simulation which requires a Hilbert space growing linearly with N .

To put the spin-wave quantum trajectories in fair comparison with the exact ones, we integrate the exact stochastic master equation (1) using the Euler-Maruyama method, and we adopt the same time step δt and the same noise realization $\delta w_i(t)$ as used in the spin-wave calculation. Note that this is a very strict benchmark as the usual Gaussian trajectory approximation for bosonic systems typically does not match the exact trajectories, as shown in [109], and the approximation is only valid in the weak sense, i.e., for calculating ensemble averages. An example of a single-trajectory benchmark for the spin-wave method is shown in Fig. 2, where we compare trajectories for both the magnetization $\langle\hat{S}^z\rangle$ and the entanglement entropy [113] S_E against exact ones. The considered system has $S = 64$ and $\omega = 1.25\kappa$, which, as predicted by the mean-field theory, corresponds to the time-crystal phase in the thermodynamical limit. The

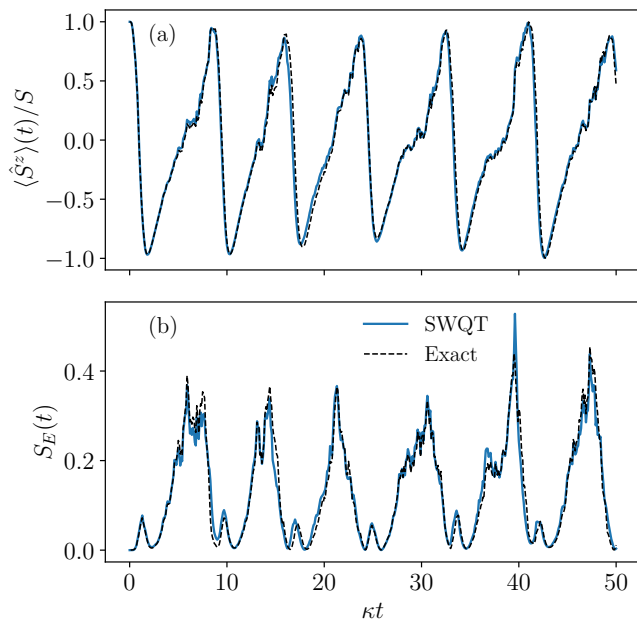


Figure 2. Single-trajectory benchmark of the spin-wave method against the exact integration of the stochastic master equation on the collective model ($\alpha = 0$). (a) The collective z -magnetization as a function of time along a single trajectory obtained from the spin-wave method (solid line) and the exact solution (dashed line). (b) The half-chain entanglement entropy along the same trajectory from the spin-wave method (solid line) and the exact solution (dashed line). Parameters: $\omega = 1.25\kappa$, $J = 0.1\kappa$, $S = 64$, $\kappa\delta t = 10^{-4}$.

initial state is the fully polarized Dicke state (all spins pointing up) for both simulations. (For the spin-wave method, this corresponds to initializing with $\theta = \phi = 0$ and $u = v = 0$.) Surprisingly, the trajectories obtained with the spin-wave method faithfully reproduce the dynamics of both quantities throughout most of the evolution. This suggests that the proposed method can be used as an approximation to resolve dynamics on the level of single trajectories.

We also evaluate the performance of the spin-wave method on trajectory-averaged quantities. Fig. 3 (a) shows the time-evolution of the spin expectations $\langle \hat{S}^{x,y,z} \rangle$ obtained by averaging spin-wave quantum trajectories. These are then benchmarked against the exact solution of the Lindblad master equation (14). As expected from the single-trajectory performance, the average dynamics is accurately reproduced. Notably, the decaying oscillations of the magnetization are due to the finite size effect and therefore require corrections beyond the mean-field level to capture. It is interesting to note that this decaying behavior is not displayed on the level of single trajectories, such as the one shown in Fig. 2 (a). This is typically observed in dissipative time crystals [114–116], and can be understood as the continuous monitoring preserving the coherence of the state. However, the different trajectories will have random relative phase shifts between

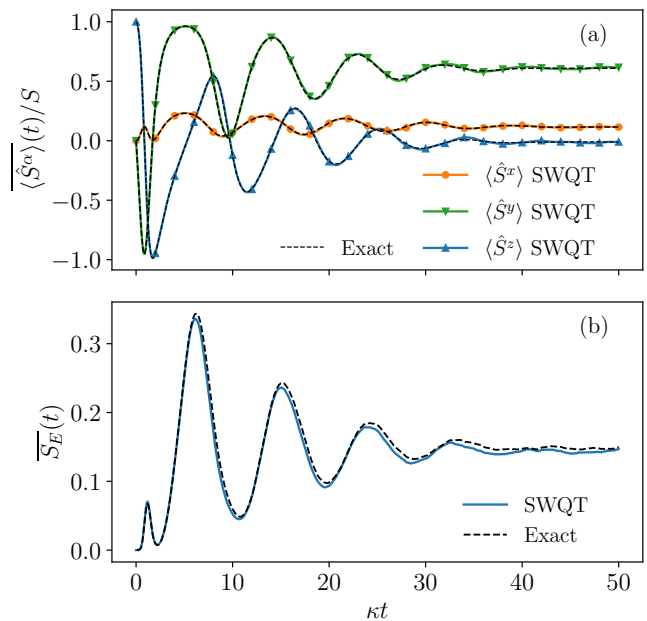


Figure 3. Benchmark of the spin-wave method on trajectory-averaged quantities. (a) Expectation of the collective spin vector \hat{S}^α as a function of time given by the spin-wave quantum trajectories (solid lines) and the exact solution of the master equation (14) (dashed lines). (b) Time-evolution of the averaged half-chain entanglement entropy from the spin-wave method (solid line) and the exact trajectories (dashed line). 4000 trajectories are used for both the spin-wave method and the exact solution of the entanglement entropy. The parameters are the same as in Fig. 2.

each other which grow with time, such that at later times the different trajectories are no longer in phase, resulting in the decaying oscillations in the averaged quantities. This also implies that the averaged state should be highly mixed, where the different components of the mixture are states close to spin coherent states pointing in different directions. The resulting mixed state is hence far from a state that can be well approximated by the lowest-order Holstein-Primakoff expansion and the Gaussian approximation as the length of the averaged collective spin vector $\langle \hat{S}^\alpha \rangle$ is only a fraction of the maximal value S . As a consequence, a deterministic version of the spin-wave theory with the same approximations applied to the averaged state, e.g., the one proposed in Ref. [97], will completely fail to capture the dynamics in this regime, cf. Appendix E for a comparison between our results and that given by the method in Ref. [97]. In Fig. 3 (b), we compare the trajectory-averaged entanglement entropy with that calculated from exact trajectories. Again, the two solutions are in good agreement, while the entanglement given by the exact simulation is slightly higher than the spin-wave results. This discrepancy is more noticeable in the presence of strong entanglement, as shown in Fig. 4, where we compare the steady-state solutions of the spin-wave method against the exact ones for a wide

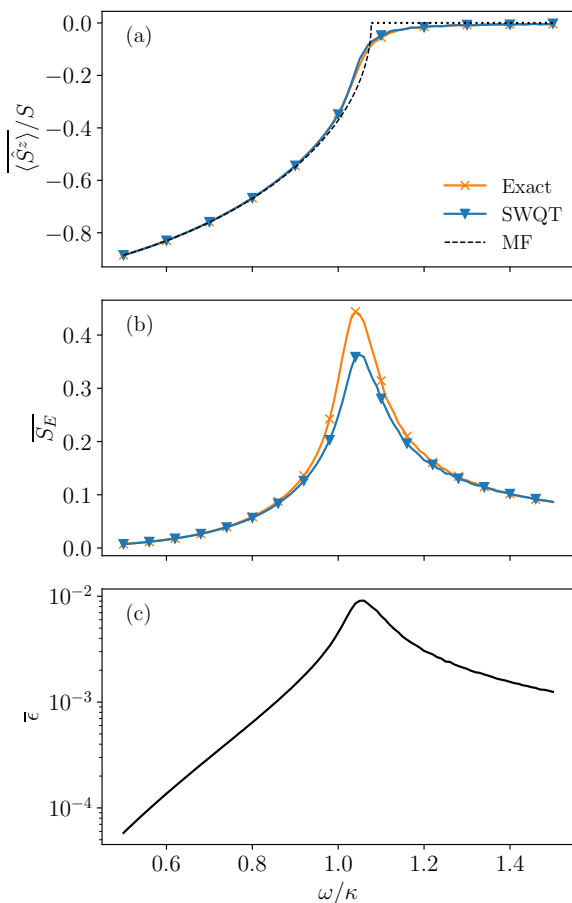


Figure 4. Benchmark of the spin-wave method on the steady state of the collective model with $S = 64$ and $J = 0.1\kappa$. (a) Expectation of the collective z -magnetization as a function of the drive ω obtained with the spin-wave quantum trajectories and the exact solution (see legend). The mean-field solution [Eq. (15)] is marked with the dashed line. (b) Trajectory-averaged steady-state half-chain entanglement entropy obtained with the two methods [see legend in (a)]. (c) Trajectory-averaged spin-wave density $\bar{\epsilon}$ in the steady state.

range of the drive ω . Fig. 4 (c) shows the trajectory-averaged steady-state spin-wave density $\bar{\epsilon}$ associated with the spin-wave solutions. The peak in $\bar{\epsilon}$ corresponds to the maximum in the entanglement entropy [in panel (b)], where the difference between the spin-wave and exact solutions is also more pronounced. This illustrates the significance of the control parameter $\bar{\epsilon}$ as a signal for the validity of the spin-wave theory. On the other hand, the qualitative behavior of the entanglement is correctly captured despite the relatively high spin-wave density at its peak, and the magnetization predicted by the spin-wave method [panel (a)] remains accurate for all values of ω considered.

B. Long-range case: $\alpha \neq 0$

To investigate the effect of a finitely long-range interaction and the entanglement dynamics in this regime, we apply the spin-wave method to the model with finite values of α . We first consider a long-range model with $\alpha = 0.2$. Fig. 5 (a) shows the steady-state expectation of the collective magnetization $\langle \hat{S}^z \rangle$ as a function of the drive amplitude ω and the system size N . As we approach the thermodynamic limit by increasing N , the spin-wave solution converges towards the mean-field prediction and a continuous transition emerges separating the normal phase with $\langle \hat{S}^z \rangle \neq 0$ and the time-crystal phase with $\langle \hat{S}^z \rangle = 0$. Fig. 5 (b) shows the behavior of the long-time-averaged half-chain entanglement entropy across this dissipative phase transition. The entanglement develops a logarithmic divergence as a function of N at the critical point (as implied by the finite-size scaling analysis of the maximum value of the entanglement entropy), while it appears to be N -independent for drive values deep inside both phases. This suggests the emergence of an entanglement phase transition separating two area-law phases. This anomaly in entanglement also corresponds to a peak in the spin-wave density, as shown in Fig. 5 (c). When the system size N increases, the spin-wave density is suppressed (including its peak value), which is a signature of the long-range nature of the model: in the $N \rightarrow \infty$ limit, a vanishing spin-wave density suggests that the system becomes equivalent to a mean-field (infinite-range) one. In Fig. 5 (d), we study the time evolution of the trajectory-averaged entanglement entropy at a driving value $\omega = 1.06\kappa$, which is close to where the maximum steady-state entanglement is achieved for the finite system sizes we studied. Note that we are increasing N exponentially between the different considered values, while the entanglement quickly reaches the steady-state value in all cases.

To study the effect of the interaction range on the entanglement dynamics, we also consider the short(er)-range case with $\alpha = 1$ for comparison. In Fig. 6 we present the same physical quantities as considered in Fig. 5 for the long-range case, whereas here we are increasing N in a linear scale between different system sizes considered. The steady-state magnetization $\langle \hat{S}^z \rangle$, as shown in Fig. 6 (a), exhibits qualitatively similar behavior to the long-range case, while it shows more deviation from the mean-field prediction. This could result from more significant finite-size effects due to short-range interactions. (Note that the mean-field theory does not account for the interaction range parameter α and therefore gives identical predictions regardless of α .) In sharp contrast, Fig. 6 (b) shows that the entanglement entropy of the short-range systems grows much faster with the system size N . Finite-size scaling suggests a volume law for the maximum entanglement entropy as well as in a vicinity around the critical point. The spin-wave density, as shown in Fig. 6 (c), also presents a qualitatively dif-

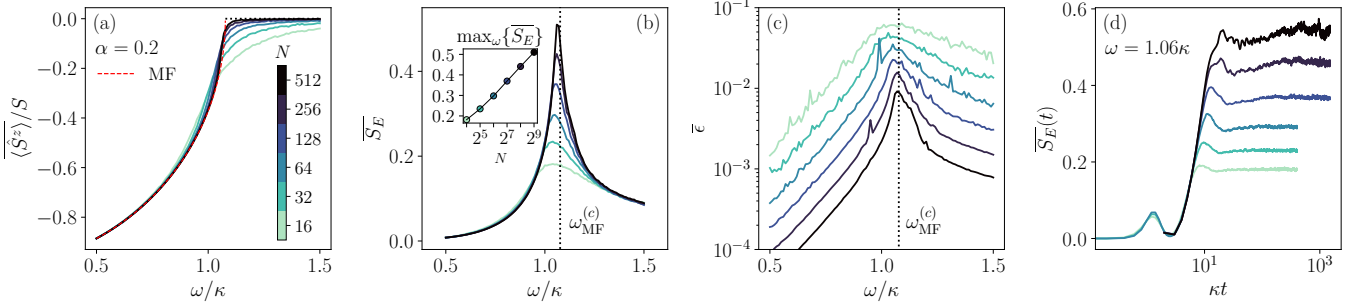


Figure 5. Results for the power-law interacting model in the long-range regime ($\alpha = 0.2$, $J = 0.1\kappa$) of different system sizes (colorbar shared across all panels). The dashed line marks the mean-field solution. (a) Steady-state average z magnetization as a function of the drive ω . (b) Steady-state of the trajectory-averaged half-chain entanglement entropy as a function of ω . The vertical dotted lines mark the critical point predicted by the mean-field theory $\omega_{\text{MF}}^{(c)} \simeq 1.077\kappa$. Inset: scaling of the maximum entropy versus N in linear-log scale. (c) Steady-state spin-wave density in log-linear scale. (d) Dynamics of the trajectory-averaged half-chain entanglement entropy for a driving value $\omega = 1.06\kappa$, in linear-log scale.

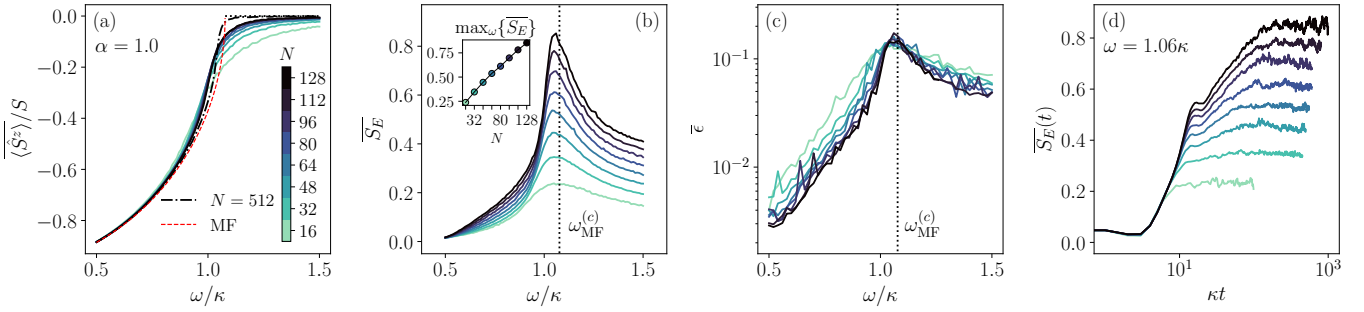


Figure 6. Results for the power-law interacting model in the short-range regime ($\alpha = 1.0$, $J = 0.1\kappa$) of different system sizes (colorbar shared across all panels). (a) Steady-state average z magnetization as a function of the drive ω . The dashed line marks the mean-field solution. (b) Steady-state of the trajectory-averaged half-chain entanglement entropy as a function of ω . The vertical dotted lines mark the critical point predicted by the mean-field theory $\omega_{\text{MF}}^{(c)} \simeq 1.077\kappa$. Inset: scaling of the maximum entropy versus N in linear scale. (c) Steady-state spin-wave density in log-linear scale. (d) Dynamics of the trajectory-averaged half-chain entanglement entropy for a driving value $\omega = 1.06\kappa$, in linear-log scale.

ferent behavior from the long-range case. Close to the maximal entanglement, the spin-wave density does not appear to decrease with the system size N , and remains around $\bar{\epsilon} \lesssim 0.2$. This suggests that the short-range model does not reduce to a mean-field (infinite-range) one even in the thermodynamic limit of $N \rightarrow \infty$, and that higher-order corrections to the theory are expected to have a more significant contribution. Finally, we show in Fig. 6 (d) the time dynamics of the trajectory-averaged entanglement entropy at $\omega = 1.06\kappa$. Contrary to the fast saturation of entanglement in the long-range (or infinite-range) regime, the time it takes to reach the steady-state value scales rapidly with N . Due to the relatively high spin-wave density at the considered driving, we expect our result to hold only qualitatively.

The results presented for both the long- and short-range cases are in qualitative agreement with the observations made in [91] although the latter are for much more modest system sizes far from the thermodynamic limit. Here, the reported results obtained with the spin-wave method are up to $N = 512$ long-range interacting

spins, which is well beyond the exactly-solvable regime. We have therefore provided much stronger evidence to support the hypothesis that entanglement phase transition persists in the considered system and exhibits fast-saturating dynamics in the presence of sufficiently long-range interactions. On the other hand, our results also suggest the breakdown of this fast saturating property in the short-range regime.

V. EXPERIMENTAL OBSERVABILITY OF MONITORED PHASES BOOSTED BY SPIN-WAVE QUANTUM TRAJECTORIES

The SWQT framework enables operational advantage in the experimental detection of monitored phases of long-range interacting systems. Compared to Ref. [91], where the post-selection overhead is mitigated by the permutation symmetry of the setup, this section described a method based on quantum-classical correlations [87, 88]. This allows to include permutation symmetry-breaking

terms, such as local measurements and power-law decaying interactions, of cornerstone importance for current quantum platforms [18–22, 117].

The stochastic dynamics governed by Eq. (1) is continuous in time, while the experimental characterization of quantum trajectories typically requires a finite temporal binning, which effectively discretizes the evolution into small time steps. Therefore, we first discuss the discretized version of the dynamics in Eq. (1) and recast it in terms of the system and ancilla degrees of freedom, a description that is particularly tailored for digital quantum simulators. Afterwards, we discuss how the SWQT allows us to substantially mitigate the post-selection within the range of applicability of the semi-classical approximations.

A. From continuous to discrete monitored dynamics

In view of the experimental implementations, for example on digital quantum simulators with discrete-time dynamics, we discuss in this subsection the discretized version of the dynamics in Eq. (1) by fixing Δt a (small) time scale of the unitary and measurement steps, which is equivalent to the continuous-time case in the limit of $\Delta t \rightarrow 0$ (see also Refs. [25, 118, 119]). As shown in Appendix A, the stochastic master equation (1) can be cast in a diagonal form such that the noises dZ_j associated with different Lindblad jump operators are independent. We consider therefore the simplified problem with a single Lindblad jump operator \hat{L} , and focus on the dissipative part of the dynamics (fixing $\hat{H} = 0$), namely

$$d\hat{\rho} = dt\mathcal{D}[\hat{L}](\hat{\rho}) + dZ^* \left(\hat{L} - \langle \hat{L} \rangle \right) \hat{\rho} + dZ \hat{\rho} \left(\hat{L}^\dagger - \langle \hat{L}^\dagger \rangle \right), \quad (47)$$

where the dissipator $\mathcal{D}[\hat{L}]$ is defined as

$$\mathcal{D}[\hat{L}](\hat{\rho}) \equiv \hat{L}\hat{\rho}\hat{L}^\dagger - \frac{1}{2} \left\{ \hat{L}^\dagger \hat{L}, \hat{\rho} \right\}, \quad (48)$$

and the zero-mean noise dZ satisfies $|dZ|^2 = dt$ and $dZ^2 = 0$. The generalization to the complete problem is then trivial.

We discretize also the range of values $dZ = (dX + idY)/\sqrt{2}$ into the finite binnings $dX \in \{-x_Q, \dots, x_Q\}$ and $dY \in \{-y_Q, \dots, y_Q\}$ for some parameter Q . The problem in Eq. (47) is then the continuous limit of some positive operator-valued measurements (POVM), which can be described using an ancilla \mathcal{A} . We fix $\Delta t > 0$ a small time-step and study the evolution as a stochastic quantum circuit. Let us consider the dynamics of the state $\hat{\mathfrak{R}}_{S,\mathcal{A}}$ describing the combined system and ancilla framework. By definition, we require that $\hat{\rho} = \text{tr}_{\mathcal{A}}(\hat{\mathfrak{R}}_{S,\mathcal{A}})$. We note that the choice of ancilla and system interaction is crucial in determining the value of dZ . For simplicity and concreteness, we consider the case of \mathcal{A} being a system of qubits, which has immediate

implementations in quantum platforms. In particular, we focus on the minimal setup of two qubits per site, each contributing respectively to the real and imaginary parts of the complex noise. This choice will fix a bimodal approximation of the Gaussian binning, namely $Q = 1$. Nevertheless, the argument below can be generalized to more involved ancillas to reproduce larger values of Q .

We denote $\mathcal{A}_{1/2}$ the ancilla qubit 1/2. The heterodyne dynamics in Eq. (47) is then generated by the system-ancilla interaction

$$\begin{aligned} \hat{U}_{S,\mathcal{A}} &= \widehat{\text{BS}} e^{\sqrt{\Delta t}(\hat{L} \otimes \hat{\sigma}_1^- - \hat{L}^\dagger \otimes \hat{\sigma}_1^+)}, \\ \widehat{\text{BS}} &= e^{\pi(\hat{\sigma}_1^+ \otimes \hat{\sigma}_2^- - \hat{\sigma}_1^- \otimes \hat{\sigma}_2^+)/4}, \end{aligned} \quad (49)$$

where \hat{L} acts on the system, $\hat{\sigma}_{1,2}^\pm$ are the uppering and lowering operators for the ancilla qubit 1 and 2 respectively, and $\widehat{\text{BS}}$ is the 50/50 beamsplitter unitary acting only on the ancilla \mathcal{A} .

Applying $\hat{U}_{S,\mathcal{A}}$ to $\hat{\mathfrak{R}}_{S,\mathcal{A}}(t) \equiv \hat{\rho}(t) \otimes |00\rangle\langle 00|$ (with the convention where $|0\rangle$ denotes the spin-up state) and projecting out \mathcal{A}_1 onto the basis $|\pm\rangle \equiv (|0\rangle \pm |1\rangle)/\sqrt{2}$ and \mathcal{A}_2 onto $|\tilde{\pm}\rangle \equiv (|0\rangle \pm i|1\rangle)/\sqrt{2}$ we have the four Kraus operators

$$\begin{aligned} \hat{K}_{\pm,\tilde{\pm}} &\equiv \langle \pm |_{\mathcal{A}_1} \langle \tilde{\pm} |_{\mathcal{A}_2} \hat{U}_{S,\mathcal{A}} |0\rangle_{\mathcal{A}_1} |0\rangle_{\mathcal{A}_2} \\ &= \frac{1}{2} \left(\mathbb{I} \pm e^{\mp \tilde{\pm} i \pi/4} \sqrt{\Delta t} \hat{L} - \frac{1}{2} \Delta t \hat{L}^\dagger \hat{L} \right), \end{aligned} \quad (50)$$

where we have kept terms up to first order in Δt . We note that the measurement information in the Kraus operators is fully encoded in the 4 complex numbers $\pm e^{\mp \tilde{\pm} i \pi/4}$. Their choice, fixing the measurement history, is therefore determined by the POVM $\hat{E}_{\pm,\tilde{\pm}} = \hat{K}_{\pm,\tilde{\pm}}^\dagger \hat{K}_{\pm,\tilde{\pm}}$. The post-measurement state is

$$\hat{\rho}_{\pm,\tilde{\pm}} = \frac{\hat{K}_{\pm,\tilde{\pm}} \hat{\rho} \hat{K}_{\pm,\tilde{\pm}}^\dagger}{p_{\pm,\tilde{\pm}}}, \quad (51)$$

where the probabilities are given by

$$p_{\pm,\tilde{\pm}} = \text{tr}(\hat{\rho} \hat{E}_{\pm,\tilde{\pm}}). \quad (52)$$

We will now briefly show that Eq. (51) reproduces Eq. (47) for small Δt , with a binary approximation of the binning. We define two stochastic variables depending on the measurement outcomes $\Delta R_x(\pm, \tilde{\pm}) \equiv \pm \sqrt{\Delta t}$ and $\Delta R_y(\pm, \tilde{\pm}) \equiv \tilde{\pm} \sqrt{\Delta t}$. We then have, at leading order in Δt , that

$$\begin{aligned} \overline{\Delta R_x} &= \sum_{\pm,\tilde{\pm}} \pm \sqrt{\Delta t} p_{\pm,\tilde{\pm}} = \Delta t \langle \hat{L}^\dagger + \hat{L} \rangle / \sqrt{2}, \\ \overline{\Delta R_y} &= \sum_{\pm,\tilde{\pm}} \tilde{\pm} \sqrt{\Delta t} p_{\pm,\tilde{\pm}} = i \Delta t \langle \hat{L}^\dagger - \hat{L} \rangle / \sqrt{2}. \end{aligned} \quad (53)$$

In a similar fashion, we have $\overline{\Delta R_x^2} = \overline{\Delta R_y^2} = \Delta t$ and $\overline{\Delta R_x \Delta R_y} = 0$. Putting all together, and defining the

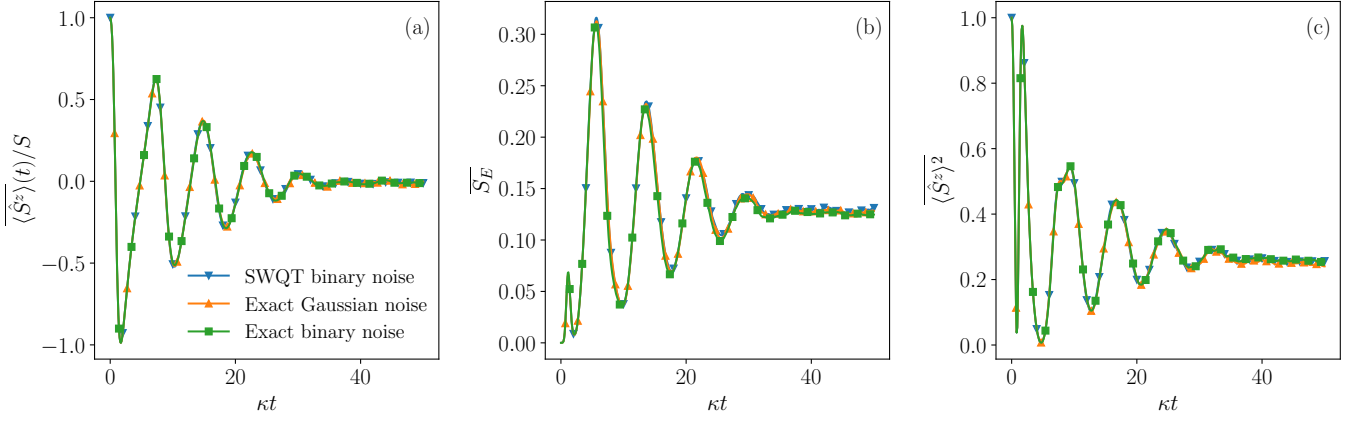


Figure 7. Benchmark of the binary approximation of the Gaussian noise in the heterodyne-detection unraveling. We compare trajectory-averaged quantities obtained from different methods and different types of noise (see legend), namely 1) the spin-wave quantum trajectory (SWQT) method with binarized noise, 2) the exact solution of the stochastic master equation with Gaussian noise and 3) the exact solution but with binary noise replacing the gaussian noise. Panel (a) compares the results on a linear quantity $\overline{\langle \hat{S}^z \rangle}$. Panel (b) and (c) show the benchmark on two different nonlinear quantities, the half-system entanglement entropy $\overline{S_E}$ and the squared magnetization $\overline{\langle \hat{S}^z \rangle^2}$ respectively. Parameters: $\omega = 1.3\kappa$, $J = 0.1\kappa$, $\alpha = 0$ and $S = 64$.

zero-mean stochastic processes $dX \equiv \Delta R_x - \overline{\Delta R_x}$ and $dY = \Delta R_y - \overline{\Delta R_y}$, which satisfy $dX^2 = dY^2 = \Delta t$ and $dXdY = 0$, we obtain the final expression after simple algebra [120],

$$\begin{aligned} \delta \hat{\rho}_{\pm, \pm} &= \hat{\rho}_{\pm, \pm} - \hat{\rho} \\ &= \Delta t \mathcal{D}[\hat{L}]\hat{\rho} + \frac{1}{\sqrt{2}} dX \left(\hat{L}\hat{\rho} + \hat{\rho}\hat{L}^\dagger - \langle \hat{L} + \hat{L}^\dagger \rangle \hat{\rho} \right) \\ &\quad + \frac{i}{\sqrt{2}} dY \left(-\hat{L}\hat{\rho} + \hat{\rho}\hat{L}^\dagger + \langle \hat{L} - \hat{L}^\dagger \rangle \hat{\rho} \right), \end{aligned} \quad (54)$$

which is equivalent to Eq. (47) when substituting $dZ = (dX + idY)/\sqrt{2}$.

We verify the validity of this binary approximation of the Gaussian noise by computing the trajectory-averaged quantities including both linear and non-linear functions of the state and compared the results with the exact solution obtained with the Gaussian noise. An example of the benchmark is shown in Fig. 7, where we computed the magnetization $\overline{\langle \hat{S}^z \rangle}$, the half-system entanglement entropy $\overline{S_E}$ and the nonlinear quantity $\overline{\langle \hat{S}^z \rangle^2}$ from three different methods: 1) Spin-wave quantum trajectories with binarized noise, 2) exact solution of the stochastic master equation with Gaussian noise and 3) exact solution with the binary approximation of the noise. In all cases, we observe excellent agreement among the results obtained in these different ways.

In summary, within the choice of ancilla and system-ancilla interaction, we obtain a 4-valued complex process dZ for each independent Lindblad jump operator \hat{L} at each monitoring step. This allows us to estimate the brute-force post-selection overhead over M discrete timesteps for Λ independent Lindblad jump operators

as $O(4^{M\Lambda})$. More generally, introducing further ancilla qubits, or enabling qubit interactions, allows one to reach a more refined binning of the Gaussian increment dZ . Fixing the binning parameter Q , the probability of reproducing the same trajectory is then $O((2Q)^{2M\Lambda})$. This renders the brute-force experimental observation of the monitored phases of generic systems an exponentially hard task.

B. Quantum-classical observables

To overcome the large post-selection overhead, we combine classical simulation with the output from a quantum simulation. We consider an experiment with $\mathcal{M} \gg 1$ (weak) measurement steps and set the measurement outcome history \mathbf{m} . As previously elaborated, the probability of obtaining \mathbf{m} twice is exponentially small in system size and time scale. Suppose we perform a final projective measurement of an operator \hat{O} over $\hat{\rho}(\mathbf{m})$, i.e. the state conditioned on the measurement history \mathbf{m} . This measurement is disruptive and will collapse $\hat{\rho}$ onto the eigenspace of the measurement outcome $o_{\mathbf{m}}$. For example, in the case where the observable is chosen to be $\hat{O} = \hat{S}^z$, the single-shot measurement outcome $o_{\mathbf{m}} \in \{-S, \dots, S\}$ is one of the $2S + 1$ eigenvalues of operator \hat{S}^z . Averaging over this value recasts the Lindblad prediction, namely $\overline{o_{\mathbf{m}}} = \text{Tr}[\hat{\rho}\hat{O}]$ where $\hat{\rho} = \hat{\rho}(\mathbf{m})$ is the average state over all possible trajectories \mathbf{m} . A correlation that is non-linear in the state can be obtained using classical simulations [87]. Fixing the measurement history and position \mathbf{m} in the classical simulation, we obtain the (classical) estimate of the trajectory-wise expectation value $\langle \hat{O}_{\mathbf{m}} \rangle_C \equiv \text{Tr}[\hat{\rho}_C(\mathbf{m})\hat{O}]$ with the label \bullet_C denoting the classically computed quantity. For instance,

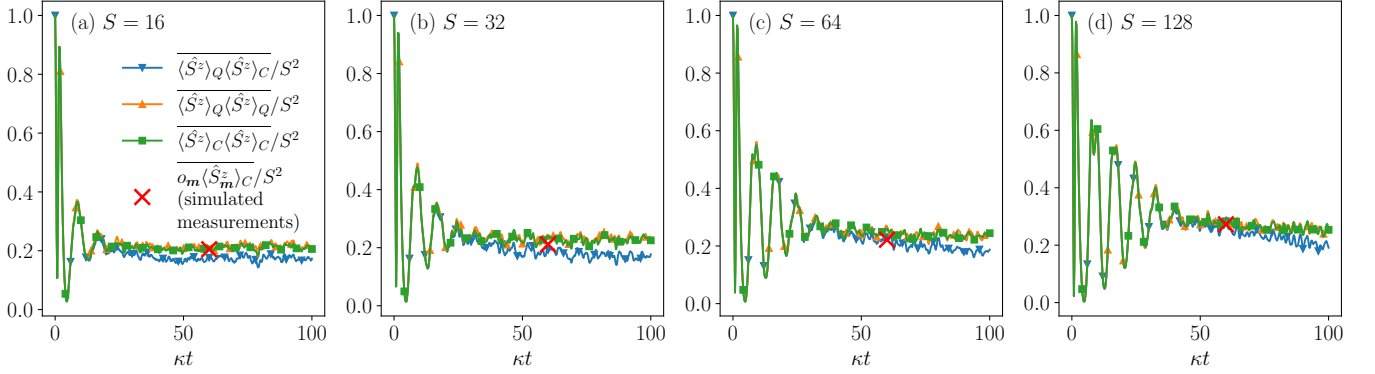


Figure 8. Benchmark of the quantum-classical measurement protocol. We compare the time evolution of the trajectory average of different correlators (see legend), the quantum-classical correlator $\langle \hat{S}^z \rangle_Q \langle \hat{S}^z \rangle_C$, the quantum-quantum correlator $\langle \hat{S}^z \rangle_Q \langle \hat{S}^z \rangle_Q$ and the classical-classical correlator $\langle \hat{S}^z \rangle_C \langle \hat{S}^z \rangle_C$. Here, trajectory-wise expectation labeled C (classical) is the spin-wave prediction, and the Q (quantum) result is given by the exact simulation with the same realization of the binary noise. The brute-force simulation of a final projective measurement at $\kappa t = 60$ is also shown (marked with a cross), where the measured results of the quantum-classical correlated probe $o_m(\hat{S}_m^z)_C$ are averaged over 480 runs of the experiment (with different noise realizations). The different panels correspond to different total spin numbers S (see annotation). Parameters: $\omega = 1.3\kappa$, $J = 0.1\kappa$.

this is obtained in our setup using the solution of Eq. (1) within the spin-wave approximations. We can then cross-correlate the measurement outcome with the classical simulation result to construct the quantum-classical object $o_m(\hat{O}_m)_C$, which, when averaged over m (i.e. over measurement shots),

$$\overline{o_m(\hat{O}_m)_C} = \overline{\langle \hat{O}_m \rangle_Q \langle \hat{O}_m \rangle_C}, \quad (55)$$

gives the quantum-classical correlator, where the label \bullet_Q denotes the quantity evaluated on the actual quantum state in the experiment. In the ideal case where the classical simulation is exact, the quantum and classical quantities should coincide and the correlator on the right-hand side of Eq. (55) is a nonlinear function of the state conditioned on the measurement history. This was recently shown to reproduce the measurement-induced transition in a variety of experiments [74], provided simulating $\langle \hat{O}_m \rangle_C$ is easy. The SWQT framework therefore is a compelling toolbox to investigate quantum-classical correlations. In particular, when the semi-classical approximation holds, we expect the data to be reliable with errors $O(1/S)$.

To benchmark this quantum-classical measurement protocol, let us consider again the infinite-range case ($\alpha = 0$) of the spin model introduced in Sec. II A, such that numerically exact integration of the stochastic master equation is affordable for sufficiently large S in order for the spin-wave approximations to yield valid results. We refer to the quantities obtained with the exact solution as the “quantum” ones, to simulate what one would get from an actual experiment. The “classical” quantities are then those given by the spin-wave solution using the same noise realization m as in the corresponding exact simulation (“quantum”) run. As justified in Sec. V A,

we adopt the binarized noise in both the exact and the spin-wave simulations, in order to mimic an experiment on discrete-time digital quantum simulators where the weak monitoring is implemented with the ancilla qubits. We fix the interaction strength to $J = 0.1\kappa$, which is the value considered in Sec. IV, and choose the observable for the final projective measurement to be $\hat{O} = \hat{S}^z$. The estimator of the statistical average $\overline{o_m(\hat{S}_m^z)_C}$ is then the quantum-classical correlator $\langle \hat{S}^z \rangle_Q \langle \hat{S}^z \rangle_C$ (we omit the subscript m for a less heavy notation). In the ideal scenario where the classical simulation is also exact as the quantum one along any trajectory, this correlator should be equal to both the classical-classical correlator $\langle \hat{S}^z \rangle_C \langle \hat{S}^z \rangle_C$ and the quantum-quantum correlator $\langle \hat{S}^z \rangle_Q \langle \hat{S}^z \rangle_Q$. In Fig. 8, we show an example of the time evolution of these three correlators at a given driving amplitude $\omega = 1.3\kappa$ for different system sizes (indicated by the total spin number S). Due to the imperfection of the spin-wave approximations along single trajectories, the quantum-classical correlator gradually deviates from the quantum-quantum and the classical-classical ones, yet still captures qualitatively the dynamics. We also show the brute force simulation result of a projective measurement at a “final” time $\kappa t = 60$, where a number of 480 shots of measurement outcomes o_m are collected and cross-correlated with the classical simulation result to construct the quantum-classical object $o_m(\hat{S}_m^z)_C$, which agrees well with its estimator $\langle \hat{S}^z \rangle_Q \langle \hat{S}^z \rangle_C$. In Fig. 9, we show the steady-state behavior of the three correlators discussed above, as a function of the drive ω for different system sizes. Importantly, the quantum-classical correlation $\langle \hat{S}^z \rangle_Q \langle \hat{S}^z \rangle_C$ successfully captures the signature of the phase transition. This demonstrates that the efficient

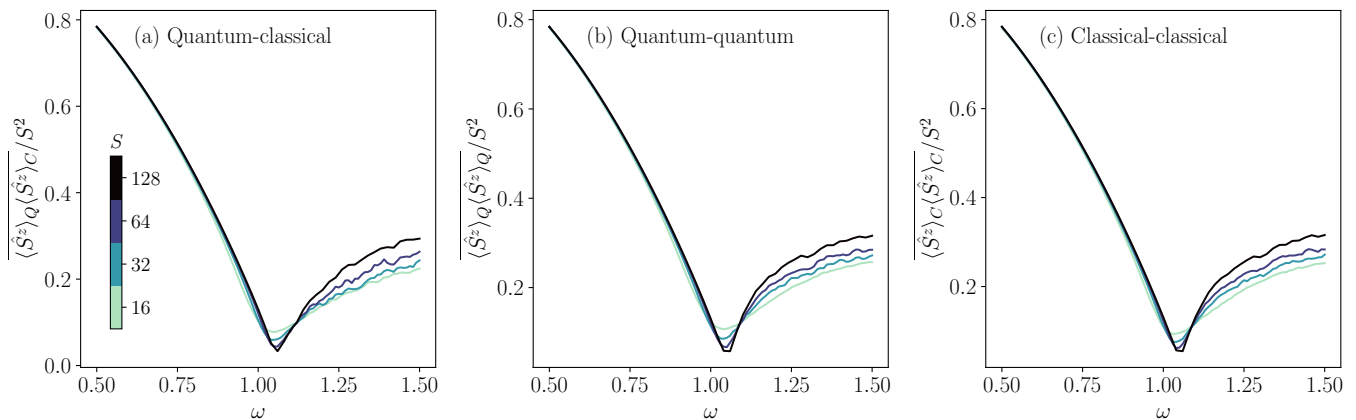


Figure 9. Steady-state trajectory-averaged correlator $\overline{\langle \hat{S}^z \rangle_Q \langle \hat{S}^z \rangle_C}$ as a function of the drive ω for different total spin numbers S (see legend). Panel (a)-(c) show the results for the the quantum-classical correlator $\langle \hat{S}^z \rangle_Q \langle \hat{S}^z \rangle_C$, the quantum-quantum correlator $\langle \hat{S}^z \rangle_Q \langle \hat{S}^z \rangle_Q$ and the classical-classical correlator $\langle \hat{S}^z \rangle_C \langle \hat{S}^z \rangle_C$ respectively. The steady-state value is computed as the average from $\kappa t = 50$ to $\kappa t = 100$, i.e. over the tail of the dynamics.

classical simulation enabled by our spin-wave framework provides access to quantum-classical observables, which can probe nonlinear properties of the state without the post-selection issue.

VI. CONCLUSIONS AND OUTLOOK

In this work, we have proposed a stochastic spin-wave theory along quantum trajectories of monitored long-range spin systems, which serves both as an algorithm for solving the Lindblad master equation and also as a method for investigating monitored dynamics on the level of trajectories with direct access to any quantity of the monitored state, such as entanglement, within the spin-wave approximations. Our technique has been carefully benchmarked in regimes where numerically exact solutions are possible, showing good accuracy even on the level of single trajectories. We further demonstrated the method on a large number of spins with power-law interactions, a regime well beyond the reach of direct simulations, and studied the entanglement dynamics in different regimes of the interaction range. Given the generality of our formalism, we expect the proposed framework of spin-wave quantum trajectories to pave the way for the investigation of a large class of long-range interacting systems.

Despite the demonstrated performance of our method, there are several interesting directions for future studies. For example, one can consider terms in the Holstein-Primakoff expansion beyond the leading order to include more nonlinear effects, which should extend the validity of the theory in the regime of relatively high spin-wave densities. We also expect better overall single-trajectory accuracy with the inclusion of higher-order spin-wave corrections, which is essential in improving the performance of the quantum-classical measurement protocol in avoid-

ing the post-selection problem. On the other hand, different unravellings of the Lindblad master equation can also be explored, including the relevant case of quantum jumps modeling the coupling to photodetectors.

The long-range spin model we adopted for the demonstration of the spin-wave theory can be readily realized in current experimental platforms [23, 121], and we expect the entanglement phase transition to be readily observable in experiments without the post-selection problem. The reason is two-fold. Firstly, as we demonstrated with the spin-wave simulations, the entanglement dynamics features fast saturation times when the interaction is sufficiently long-range, which, together with the collective nature of the dissipation, allows the brute-force post-selection of quantum trajectories with a mitigated, non-exponential, overhead. Finally, in a much broader context, when the semi-classical approximations are valid – including the relevant case of sufficiently long-range interactions, the efficient classical simulation of spin-wave quantum trajectories allows to probe nonlinear quantities of the state via quantum-classical cross-correlated observables, which does not suffer from the post-selection problem, thus opening up promising avenues in the experimental detection of monitored phases in long-range systems.

ACKNOWLEDGMENTS

We would like to thank Marco Schirò, Gerald E. Fux, Procolo Lucignano, Gianluca Passarelli, Silvia Pappalardi, Cristiano Ciuti, and Valentin Heyraud for helpful discussions. This work was supported by PNRR MUR project PE0000023- NQSTI, by the European Union (ERC, RAVE, 101053159). X.T. acknowledges support from DFG under Germany’s Excellence Strategy – Cluster of Excellence Matter and Light for Quantum Com-

puting (ML4Q) EXC 2004/1 – 390534769, and DFG Collaborative Research Center (CRC) 183 Project No. 277101999 - project B01. Views and opinions expressed are however those of the author(s) only and do not necessarily reflect those of the European Union or the European Research Council. Neither the European Union nor the granting authority can be held responsible for them.

Appendix A: Proof of the unraveling of the nondiagonal Lindblad master equation

The positive semidefinite matrix f_{ij} in the nondiagonal master equation (6) can be diagonalized with a unitary transformation u :

$$f = u\kappa u^\dagger, \quad (\text{A1})$$

where κ is a diagonal matrix with non-negative entries:

$$\kappa \equiv \text{diag}(\kappa_1, \dots, \kappa_N). \quad (\text{A2})$$

Defining

$$\begin{aligned} \hat{A}_i &\equiv \sum_j u_{ji} \hat{L}_j, \\ dZ_i &\equiv \frac{1}{\sqrt{\kappa_i}} \sum_j u_{ji} dw_j, \end{aligned} \quad (\text{A3})$$

the Liouvillian (6) becomes

$$\mathcal{L}(\hat{\rho}) = -i[\hat{H}, \hat{\rho}] + \sum_i \kappa_i \mathcal{D}[\hat{A}_i](\hat{\rho}), \quad (\text{A4})$$

where

$$\mathcal{D}[\hat{A}_i](\hat{\rho}) \equiv \hat{A}_i \hat{\rho} \hat{A}_i^\dagger - \frac{1}{2} \left\{ \hat{A}_i^\dagger \hat{A}_i, \hat{\rho} \right\} \quad (\text{A5})$$

is the standard (diagonal) dissipator. The unraveling (1) becomes

$$\begin{aligned} d\hat{\rho} &= dt \mathcal{L}(\hat{\rho}) \\ &+ \sum_i \sqrt{\kappa_i} \left[dZ_i^* \left(\hat{A}_j - \langle \hat{A}_i \rangle \right) \hat{\rho} + dZ_i \hat{\rho} \left(\hat{A}_i^\dagger - \langle \hat{A}_i^\dagger \rangle \right) \right], \end{aligned} \quad (\text{A6})$$

where the noise satisfies

$$\begin{aligned} \overline{dZ_i} &= 0, \\ dZ_i^* dZ_j &= \delta_{ij} dt, \quad dZ_i dZ_j = 0, \end{aligned} \quad (\text{A7})$$

which implies that each dZ_i is a normalized complex Wiener process and independent from each other. Eq. (A6), being equivalent to Eq. (1), is the standard (diagonal-form) quantum state diffusion unraveling describing a heterodyne detection process, where the operators \hat{A}_i are being continuously monitored at rates κ_i respectively.

For a pure initial state, this is equivalent to the following stochastic Schrödinger equation,

$$\begin{aligned} d|\psi\rangle &= -i\hat{H}dt|\psi\rangle \\ &+ \sum_i \kappa_i \left(\langle \hat{A}_i^\dagger \rangle \hat{A}_i - \frac{1}{2} \langle \hat{A}_i^\dagger \rangle \langle \hat{A}_i \rangle - \frac{1}{2} \hat{A}_i^\dagger \hat{A}_i \right) dt |\psi\rangle \\ &+ \sum_i \sqrt{\kappa_i} \left(\hat{A}_i - \langle \hat{A}_i \rangle \right) dZ_i^* |\psi\rangle, \end{aligned} \quad (\text{A8})$$

which preserves the purity of the state along every single trajectory.

Appendix B: Mean-field equations for the power-law spin model

We derive in this appendix the mean-field equations of the power-law spin model defined in Sec. II A. We denote the average magnetization with

$$m_\mu \equiv \frac{\langle \hat{S}^\mu \rangle}{S} = \frac{1}{N} \sum_{i=1}^N \langle \hat{\sigma}_i^\mu \rangle, \quad \mu \in \{x, y, z\}, \quad (\text{B1})$$

whose evolution under the Lindblad dynamics can be obtained with the adjoint master equation [122]: for a time-independent operator \hat{O} , we have

$$\frac{d\langle \hat{O} \rangle}{dt} = i \langle [\hat{H}, \hat{O}] \rangle + \frac{\kappa}{S} \left\langle \hat{S}^+ \hat{O} \hat{S}^- - \frac{1}{2} \left\{ \hat{S}^+ \hat{S}^-, \hat{O} \right\} \right\rangle. \quad (\text{B2})$$

Within the mean-field approximation, where we assume the factorization $\langle \hat{\sigma}_i^\mu \hat{\sigma}_j^\lambda \rangle = \langle \hat{\sigma}_i^\mu \rangle \langle \hat{\sigma}_j^\lambda \rangle$ at $N \rightarrow \infty$, and that $\langle \hat{\sigma}_i^\mu \rangle$ has no i -dependence, we obtain the following equations of motion for the average magnetization:

$$\begin{aligned} \frac{dm_x}{dt} &= -4Jm_y m_z + \kappa m_x m_z, \\ \frac{dm_y}{dt} &= -\omega m_z + 4Jm_x m_z + \kappa m_y m_z, \\ \frac{dm_z}{dt} &= \omega m_y - \kappa(m_x^2 + m_y^2). \end{aligned} \quad (\text{B3})$$

The steady-state magnetization can be found by imposing the time derivatives to zero, which yields

$$m_z = -\sqrt{1 - \frac{\omega^2}{16J^2 + \kappa^2}}, \quad (\text{B4})$$

giving Eq. (15) in the main text. Beyond the critical point $\omega_{\text{MF}}^{(c)} = \sqrt{16J^2 + \kappa^2}$, this stationary solution no longer exists and the magnetization admits only permanently oscillating solutions, which corresponds to a time-crystal phase.

Appendix C: Expression for the entanglement entropy under the Gaussian approximation

Without loss of generality, let us consider a bipartition of the spins where one subsystem contains spins indexed

from 1 to M . Denoting $\hat{x}_i \equiv (\hat{b}_i^\dagger + \hat{b}_i)/\sqrt{2}$, $\hat{p}_i \equiv i(\hat{b}_i^\dagger - \hat{b}_i)/\sqrt{2}$ and $\hat{\mathbf{r}} \equiv (\hat{x}_1, \dots, \hat{x}_M, \hat{p}_1, \dots, \hat{p}_M)$, the covariance matrix Ξ for the Gaussian state of the subsystem has components

$$\Xi_{ij} \equiv \frac{1}{2} \langle \hat{r}_i \hat{r}_j + \hat{r}_j \hat{r}_i \rangle - \langle \hat{r}_i \rangle \langle \hat{r}_j \rangle, \quad (\text{C1})$$

which can be expressed in terms of u_{ij} and v_{ij} . The entanglement entropy S_E is then given by the von Neumann entropy of the subsystem (since the full system remains in a pure state along the unraveled trajectory), which can be expressed in terms of the symplectic eigenvalues $\{\mu_i\}_i$ of the covariance matrix Ξ as [111]

$$S_E = \sum_i \left[\left(\mu_i + \frac{1}{2} \right) \log \left(\mu_i + \frac{1}{2} \right) - \left(\mu_i - \frac{1}{2} \right) \log \left(\mu_i - \frac{1}{2} \right) \right]. \quad (\text{C2})$$

Operationally, the symplectic eigenvalues can be found with the help of the symplectic matrix Ω defined as

$$\Omega = \begin{pmatrix} \mathbf{0} & \mathbf{I}_M \\ -\mathbf{I}_M & \mathbf{0} \end{pmatrix}, \quad (\text{C3})$$

where \mathbf{I}_M is the $M \times M$ identity matrix. The eigenvalues of the matrix $\Xi\Omega$ are then $\{\pm i\mu_i\}_i$, where the μ_i 's are the symplectic eigenvalues of Ξ .

Appendix D: Generalization to spin-boson systems

In this appendix, we demonstrate a possible extension of our spin-wave theory, which allows the investigation of spin-boson systems. We adopt the same Gaussian approximation for the bosonic mode as for the bosonized spins, such that the state of the entire system can be characterized by the first and second moments, requiring a quadratic number of variables to specify the Gaussian variational ansatz in the general case. For illustration purposes, let us consider a driven-dissipative Tavis-Cummings model with long-range spin interactions. The spins are collectively driven and resonantly coupled to a single-mode cavity (with annihilation operator \hat{a} for the cavity bosonic mode), and the cavity undergoes single-photon dissipation. The Hamiltonian can be written as follows,

$$\hat{H} = \omega \hat{S}^x + \frac{2sJ}{\mathcal{N}} \sum_{i \neq j} \frac{\hat{\sigma}_i^z \hat{\sigma}_j^z}{d(i,j)^\alpha} + \frac{\lambda}{\sqrt{2S}} (\hat{a}^\dagger \hat{S}^- + \hat{a} \hat{S}^+), \quad (\text{D1})$$

Which is essentially the spin Hamiltonian (7) with an additional term (in the second line) describing the spin-boson coupling (with strength λ). The average dynamics

of the system can be described by the Lindblad master equation,

$$\frac{d}{dt} \hat{\rho} = -i[\hat{H}, \hat{\rho}] + \kappa \mathcal{D}[\hat{a}](\hat{\rho}), \quad (\text{D2})$$

where κ represents the loss rate of the cavity photons.

Let us consider the same quantum-state diffusion unraveling as in the main text. For a time-independent operator \hat{O} , the stochastic evolution of its expectation is given by

$$d\langle \hat{O} \rangle = \text{idt} \langle [\hat{H}, \hat{O}] \rangle + \kappa dt \left\langle \hat{a}^\dagger \hat{O} \hat{a} - \frac{1}{2} \left\{ \hat{a}^\dagger \hat{a}, \hat{O} \right\} \right\rangle + \sqrt{\kappa} \left\{ dZ^* \left(\langle \hat{O} \hat{a} \rangle - \langle \hat{O} \rangle \langle \hat{a} \rangle \right) + dZ \left(\langle \hat{a}^\dagger \hat{O} \rangle - \langle \hat{a}^\dagger \rangle \langle \hat{O} \rangle \right) \right\}, \quad (\text{D3})$$

where the single-channel noise dZ satisfies $dZ^2 = 0$ and $|dZ|^2 = dt$. This corresponds to monitoring the cavity output field with a heterodyne-detection scheme.

1. Equations of motion

As our model preserves the translational symmetry of the state on the level of single trajectories, within the Gaussian approximation for both the cavity and the spins, we only need to keep track of the following quantities to fully specify the state:

- First moments: $\alpha \equiv \langle \hat{a} \rangle$, $\beta \equiv \langle \hat{b}_{n_0} \rangle$ (where n_0 is an arbitrary spin index, whose value has no importance due to the translational invariance of the spins.).
- Second moments:
 - Photon-photon correlations: $u^{(a)} \equiv \langle \hat{\delta}^{(a)} \hat{\delta}^{(a)} \rangle$, $v^{(a)} \equiv \langle \hat{\delta}^{(a)\dagger} \hat{\delta}^{(a)} \rangle$.
 - Photon-spin correlations: $u^{(ab)} \equiv \langle \hat{\delta}^{(a)} \hat{\delta}_{n_0}^{(b)} \rangle$, $v^{(ab)} \equiv \langle \hat{\delta}^{(a)\dagger} \hat{\delta}_{n_0}^{(b)} \rangle$.
 - Spin-spin correlations: $u_m^{(b)} \equiv \langle \hat{\delta}_{n_0}^{(b)} \hat{\delta}_{n_0+m}^{(b)} \rangle$, $v_m^{(b)} \equiv \langle \hat{\delta}_{n_0}^{(b)\dagger} \hat{\delta}_{n_0+m}^{(b)} \rangle$.

Here, we define $\hat{\delta}^{(a)} \equiv \hat{a} - \langle \hat{a} \rangle$ and $\hat{\delta}_i^{(b)} \equiv \hat{b}_i - \langle \hat{b}_i \rangle$, which are time-dependent operators. The spin correlators satisfy $u_m^{(b)} = u_{-m}^{(b)}$ and $v_m^{(b)} = v_{-m}^{(b)}$ due to spatial reflection symmetry in the considered model.

In the re-alignment step, as the rotation applies only to the spin operators, the cavity mode is not affected. Therefore, after obtaining the angular increments $\Delta\theta$ and $\Delta\phi$ from the incremented β using Eq. (42) in the main text, We have the following update rules,

$$\begin{aligned} \beta &\leftarrow 0, \\ u^{(ab)} &\leftarrow u^{(ab)} e^{-i\Delta\phi \cos \theta}, \\ v^{(ab)} &\leftarrow v^{(ab)} e^{-i\Delta\phi \cos \theta}, \\ u_m^{(b)} &\leftarrow u_m^{(b)} e^{-2i\Delta\phi \cos \theta}, \end{aligned} \quad (\text{D4})$$

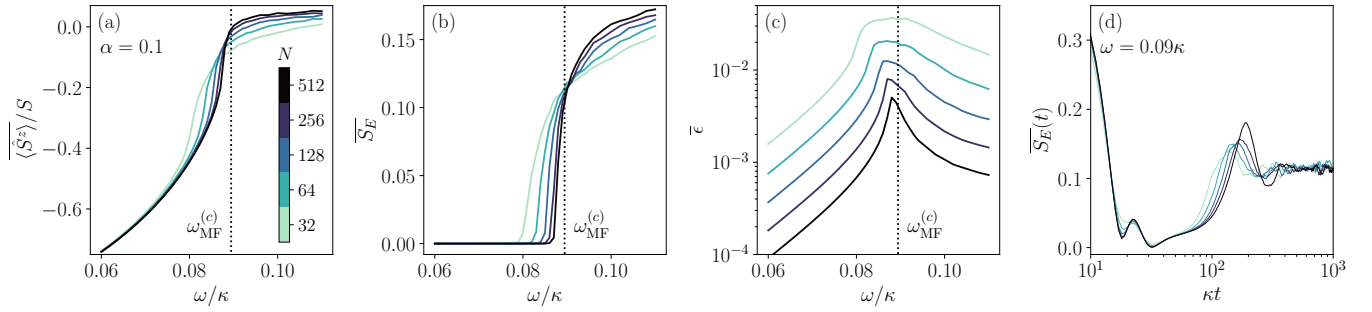


Figure 10. Results for the power-law interacting Tavis-Cummings model with $\alpha = 0.1$, $J = 0.01\kappa$ and $\lambda = 0.2\kappa$ of different system sizes (colorbar shared across all panels). (a) Steady-state average z magnetization as a function of the drive ω . The vertical dotted line marks the critical point predicted by the mean-field theory $\omega_{\text{MF}}^{(c)} \simeq 0.089\kappa$. (b) Steady-state of the trajectory-averaged entanglement entropy (between the spins and the cavity) as a function of ω . (c) Steady-state spin-wave density. (d) Dynamics of the trajectory-averaged spin-cavity entanglement entropy for a driving value $\omega = 0.09\kappa$, in linear-log scale.

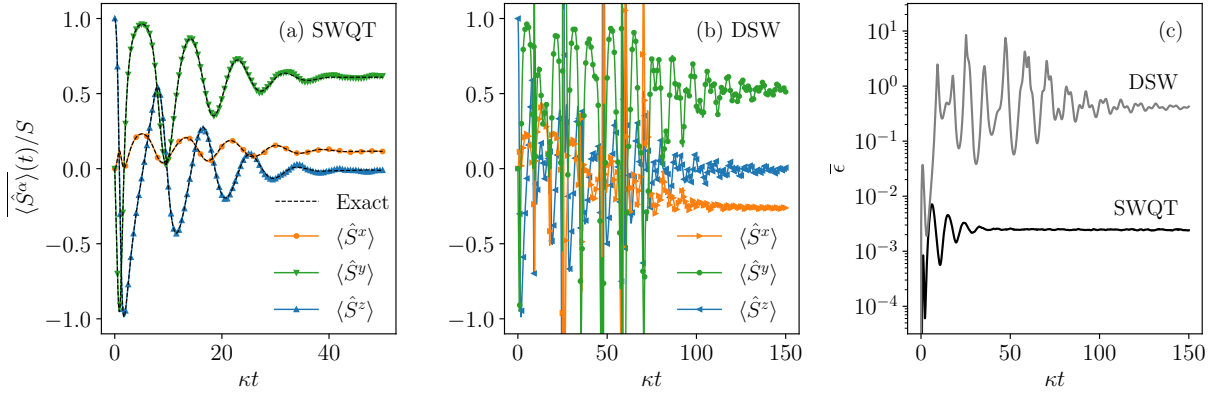


Figure 11. Comparison between solutions given by the two different spin-wave methods. (a) Results from the spin-wave quantum trajectories (SWQT) on the expectation value of the collective spin vector in the time-crystal regime with parameters $\omega_F = 1.25\kappa$, $J = 0.1\kappa$ and $S = 64$ (the same as Fig. 3). (b) The solution given by the deterministic spin-wave theory (DSW) with the same parameters. (c) Spin-wave densities associated with the two solutions.

and the other correlators remain unchanged.

2. Results on the driven-dissipative long-range Tavis-Cummings model

Note that in the regime where the cavity dissipation is much faster than any other time scale in the system, i.e. when $\omega, J, \lambda \ll \kappa$, the cavity mode can be adiabatically eliminated and this model reduces effectively to the long-range spin model with collective spin dissipation \hat{S}^- as considered in the main text, since the lossy cavity acts as a Markovian reservoir for the spin system that quickly evacuates entropy into the environment via the spin-boson interaction. To illustrate the generalization of our spin-wave quantum trajectory method to spin-boson systems, we place ourselves close to this regime, such that results qualitatively reminiscent of those in the spin-only model as presented in the main text can be expected. We fix the parameters as $s = 1/2$, $\lambda = 0.2\kappa$, $J = 0.01\kappa$ and $\alpha = 0.1$, and the results are shown in

Fig. 10. The spin magnetization [panel (a)] displays similar behavior as compared to Fig. 5 (a), where a continuous dissipative phase transition predicted by the mean-field theory emerges. This transition is also accompanied by an entanglement phase transition [panel (b)] for the entanglement between the spins and the cavity, from an unentangled phase to an entangled one as the driving increases. The spin-wave density [panel (c)] displays a maximum close to the critical point, while the peak value decreases with the system size N , which is a signature of the long-range nature of the system. Finally, the spin-cavity entanglement also exhibits fast saturation, as shown in panel (d) for the case close to criticality. These results suggest a possible implementation of the long-range spin model with collective dissipation (as considered in the main text) in atom-cavity platforms, and that the brute-force experimental detection of the entanglement phase transition can also be realized with mitigated post-selection overhead.

Appendix E: Comparison with other existing spin-wave methods

In this appendix, we provide a comparison between our method of spin-wave quantum trajectories (SWQT) and the method proposed in [97], which is a deterministic spin-wave method for dissipative systems (referred to as “DSW” in this section). The latter assumes the same approximations as in our method (i.e. lowest-order Holstein-Primakoff expansion and Gaussian approximation) except that their approximations are performed on the level of the averaged state (i.e. the density matrix) and their dynamical evolution is derived from the deterministic Lindblad master equation.

For illustration purposes, let us consider again the col-

lective spin model defined in Sec. IV of the main text. The solutions given by the two methods are shown in Fig. 11 for comparison. Panel (a) shows the SWQT results for the parameters $\omega_F = 1.25\kappa$, $J = 0.1\kappa$, $S = 64$, which is the same as that presented in Fig. 3 of the main text. The solution with the same parameters given by DSW is shown in panel (b), which is by no means close to the exact solution. As explained in the main text, this is a result of the highly mixed nature of the average state that the spin-wave approximations fail to capture. Panel (c) shows the spin-wave densities associated with the two solutions, where the SWQT has a spin-wave density that is smaller by several orders of magnitude, which is consistent with its accuracy compared to the exact solution.

-
- [1] N. Defenu, T. Donner, T. Macrì, G. Pagano, S. Ruffo, and A. Trombettoni, Long-range interacting quantum systems, *Rev. Mod. Phys.* **95**, 035002 (2023).
 - [2] N. Defenu, A. Lerose, and S. Pappalardi, Out-of-equilibrium dynamics of quantum many-body systems with long-range interactions, *Phys. Rep.* **1074**, 1 (2024).
 - [3] W. Dür, L. Hartmann, M. Hein, M. Lewenstein, and H.-J. Briegel, Entanglement in Spin Chains and Lattices with Long-Range Ising-Type Interactions, *Phys. Rev. Lett.* **94**, 097203 (2005).
 - [4] J. Eisert, M. Van Den Worm, S. R. Manmana, and M. Kastner, Breakdown of Quasilocality in Long-Range Quantum Lattice Models, *Phys. Rev. Lett.* **111**, 260401 (2013).
 - [5] P. Hauke and L. Tagliacozzo, Spread of Correlations in Long-Range Interacting Quantum Systems, *Phys. Rev. Lett.* **111**, 207202 (2013).
 - [6] P. Richerme, Z.-X. Gong, A. Lee, C. Senko, J. Smith, M. Foss-Feig, S. Michalakis, A. V. Gorshkov, and C. Monroe, Non-local propagation of correlations in quantum systems with long-range interactions, *Nature* **511**, 198 (2014).
 - [7] A. Lerose and S. Pappalardi, Origin of the slow growth of entanglement entropy in long-range interacting spin systems, *Phys. Rev. Res.* **2**, 012041 (2020).
 - [8] A. Lerose and S. Pappalardi, Bridging entanglement dynamics and chaos in semiclassical systems, *Phys. Rev. A* **102**, 032404 (2020).
 - [9] M. Antoni and S. Ruffo, Clustering and relaxation in Hamiltonian long-range dynamics, *Phys. Rev. E* **52**, 2361 (1995).
 - [10] M. Kastner, Diverging Equilibration Times in Long-Range Quantum Spin Models, *Phys. Rev. Lett.* **106**, 130601 (2011).
 - [11] S. Gupta and D. Mukamel, Slow Relaxation in Long-Range Interacting Systems with Stochastic Dynamics, *Phys. Rev. Lett.* **105**, 040602 (2010).
 - [12] S. Pappalardi, A. Russomanno, B. Žunkovič, F. Iemini, A. Silva, and R. Fazio, Scrambling and entanglement spreading in long-range spin chains, *Phys. Rev. B* **98**, 134303 (2018).
 - [13] C.-F. Chen and A. Lucas, Finite Speed of Quantum Scrambling with Long Range Interactions, *Phys. Rev. Lett.* **123**, 250605 (2019).
 - [14] M. K. Joshi, A. Elben, B. Vermersch, T. Brydges, C. Maier, P. Zoller, R. Blatt, and C. F. Roos, Quantum Information Scrambling in a Trapped-Ion Quantum Simulator with Tunable Range Interactions, *Phys. Rev. Lett.* **124**, 240505 (2020).
 - [15] D. Mukamel, S. Ruffo, and N. Schreiber, Breaking of Ergodicity and Long Relaxation Times in Systems with Long-Range Interactions, *Phys. Rev. Lett.* **95**, 240604 (2005).
 - [16] P. Kubala, P. Sierant, G. Morigi, and J. Zakrzewski, Ergodicity breaking with long-range cavity-induced quasiperiodic interactions, *Phys. Rev. B* **103**, 174208 (2021).
 - [17] P. Hauke and M. Heyl, Many-body localization and quantum ergodicity in disordered long-range Ising models, *Phys. Rev. B* **92**, 134204 (2015).
 - [18] C. Monroe, W. C. Campbell, L.-M. Duan, Z.-X. Gong, A. V. Gorshkov, P. W. Hess, R. Islam, K. Kim, N. M. Linke, G. Pagano, P. Richerme, C. Senko, and N. Y. Yao, Programmable quantum simulations of spin systems with trapped ions, *Rev. Mod. Phys.* **93**, 025001 (2021).
 - [19] H. Ritsch, P. Domokos, F. Brennecke, and T. Esslinger, Cold atoms in cavity-generated dynamical optical potentials, *Rev. Mod. Phys.* **85**, 553 (2013).
 - [20] T. Lahaye, C. Menotti, L. Santos, M. Lewenstein, and T. Pfau, The physics of dipolar bosonic quantum gases, *Rep. Prog. Phys.* **72**, 126401 (2009).
 - [21] J. L. Bohn, A. M. Rey, and J. Ye, Cold molecules: Progress in quantum engineering of chemistry and quantum matter, *Science* **357**, 1002 (2017).
 - [22] H. Weimer, M. Müller, I. Lesanovsky, P. Zoller, and H. P. Büchler, A rydberg quantum simulator, *Nat. Phys.* **6**, 382 (2010).
 - [23] G. Ferioli, A. Glicenstein, I. Ferrier-Barbut, and A. Browaeys, A non-equilibrium superradiant phase transition in free space, *Nat. Phys.* **19**, 1345 (2023).
 - [24] M. B. Plenio and P. L. Knight, The quantum-jump approach to dissipative dynamics in quantum optics, *Rev. Mod. Phys.* **70**, 101 (1998).
 - [25] H. M. Wiseman and G. J. Milburn, *Quantum measurement and control* (Cambridge university press, 2009).

- [26] H. Carmichael, *Statistical Methods in Quantum Optics 2: Non-Classical Fields*, Theoretical and Mathematical Physics (Springer Berlin Heidelberg, 2010).
- [27] K. Jacobs, *Quantum Measurement Theory and its Applications* (Cambridge University Press, 2014).
- [28] A. J. Daley, Quantum trajectories and open many-body quantum systems, *Adv. Phys.* **63**, 77–149 (2014).
- [29] B. Skinner, J. Ruhman, and A. Nahum, Measurement-induced phase transitions in the dynamics of entanglement, *Phys. Rev. X* **9**, 031009 (2019).
- [30] Y. Li, X. Chen, and M. P. A. Fisher, Quantum zeno effect and the many-body entanglement transition, *Phys. Rev. B* **98**, 205136 (2018).
- [31] X. Cao, A. Tilloy, and A. D. Luca, Entanglement in a fermion chain under continuous monitoring, *SciPost Phys.* **7**, 024 (2019).
- [32] A. C. Potter and R. Vasseur, Entanglement dynamics in hybrid quantum circuits, in *Entanglement in Spin Chains* (Springer International Publishing, 2022) p. 211–249.
- [33] M. P. Fisher, V. Khemani, A. Nahum, and S. Vijay, Random quantum circuits, *Ann. Rev. Cond. Mat. Phys.* **14**, 335–379 (2023).
- [34] Y. Li, X. Chen, and M. P. A. Fisher, Measurement-driven entanglement transition in hybrid quantum circuits, *Phys. Rev. B* **100**, 134306 (2019).
- [35] C.-M. Jian, Y.-Z. You, R. Vasseur, and A. W. W. Ludwig, Measurement-induced criticality in random quantum circuits, *Phys. Rev. B* **101**, 104302 (2020).
- [36] A. Zabalo, M. J. Gullans, J. H. Wilson, S. Gopalakrishnan, D. A. Huse, and J. H. Pixley, Critical properties of the measurement-induced transition in random quantum circuits, *Phys. Rev. B* **101**, 060301 (2020).
- [37] A. Zabalo, M. J. Gullans, J. H. Wilson, R. Vasseur, A. W. W. Ludwig, S. Gopalakrishnan, D. A. Huse, and J. H. Pixley, Operator scaling dimensions and multifractality at measurement-induced transitions, *Phys. Rev. Lett.* **128**, 050602 (2022).
- [38] P. Sierant and X. Turkeshi, Universal behavior beyond multifractality of wave functions at measurement-induced phase transitions, *Phys. Rev. Lett.* **128**, 130605 (2022).
- [39] P. Sierant, M. Schirò, M. Lewenstein, and X. Turkeshi, Measurement-induced phase transitions in $(d + 1)$ -dimensional stabilizer circuits, *Phys. Rev. B* **106**, 214316 (2022).
- [40] M. Ippoliti and V. Khemani, Postselection-free entanglement dynamics via spacetime duality, *Phys. Rev. Lett.* **126**, 060501 (2021).
- [41] M. Ippoliti, T. Rakovszky, and V. Khemani, Fractal, logarithmic, and volume-law entangled nonthermal steady states via spacetime duality, *Phys. Rev. X* **12**, 011045 (2022).
- [42] T.-C. Lu and T. Grover, Spacetime duality between localization transitions and measurement-induced transitions, *PRX Quantum* **2**, 040319 (2021).
- [43] O. Alberton, M. Buchhold, and S. Diehl, Entanglement transition in a monitored free-fermion chain: From extended criticality to area law, *Phys. Rev. Lett.* **126**, 170602 (2021).
- [44] M. Buchhold, Y. Minoguchi, A. Altland, and S. Diehl, Effective theory for the measurement-induced phase transition of dirac fermions, *Phys. Rev. X* **11**, 041004 (2021).
- [45] C.-M. Jian, H. Shapourian, B. Bauer, and A. W. W. Ludwig, (2023), [arXiv:2302.09094](https://arxiv.org/abs/2302.09094) [[cond-mat.stat-mech](https://arxiv.org/abs/2302.09094)].
- [46] M. Fava, L. Piroli, T. Swann, D. Bernard, and A. Nahum, Nonlinear sigma models for monitored dynamics of free fermions, *Phys. Rev. X* **13**, 041045 (2023).
- [47] X. Turkeshi, A. Biella, R. Fazio, M. Dalmonte, and M. Schirò, Measurement-induced entanglement transitions in the quantum ising chain: From infinite to zero clicks, *Phys. Rev. B* **103**, 224210 (2021).
- [48] X. Turkeshi, M. Dalmonte, R. Fazio, and M. Schirò, Entanglement transitions from stochastic resetting of non-hermitian quasiparticles, *Phys. Rev. B* **105**, L241114 (2022).
- [49] H. Lóio, A. De Luca, J. De Nardis, and X. Turkeshi, Purification timescales in monitored fermions, *Phys. Rev. B* **108**, L020306 (2023).
- [50] I. Poboiko, P. Pöpperl, I. V. Gornyi, and A. D. Mirlin, Theory of free fermions under random projective measurements, *Phys. Rev. X* **13**, 041046 (2023).
- [51] K. Chahine and M. Buchhold, (2023), [arXiv:2309.12391](https://arxiv.org/abs/2309.12391) [[cond-mat.str-el](https://arxiv.org/abs/2309.12391)].
- [52] E. Tirrito, A. Santini, R. Fazio, and M. Collura, Full counting statistics as probe of measurement-induced transitions in the quantum Ising chain, *SciPost Phys.* **15**, 096 (2023).
- [53] G. Kells, D. Meidan, and A. Romito, Topological transitions in weakly monitored free fermions, *SciPost Phys.* **14**, 031 (2023).
- [54] Y. L. Gal, X. Turkeshi, and M. Schirò, (2024), [arXiv:2312.13419](https://arxiv.org/abs/2312.13419) [[cond-mat.stat-mech](https://arxiv.org/abs/2312.13419)].
- [55] A. Paviglianiti and A. Silva, Multipartite entanglement in the measurement-induced phase transition of the quantum ising chain, *Phys. Rev. B* **108**, 184302 (2023).
- [56] Y. Fuji and Y. Ashida, Measurement-induced quantum criticality under continuous monitoring, *Phys. Rev. B* **102**, 054302 (2020).
- [57] O. Lunt and A. Pal, Measurement-induced entanglement transitions in many-body localized systems, *Phys. Rev. Res.* **2**, 043072 (2020).
- [58] A. Altland, M. Buchhold, S. Diehl, and T. Micklitz, Dynamics of measured many-body quantum chaotic systems, *Phys. Rev. Res.* **4**, L022066 (2022).
- [59] L. Lumia, E. Tirrito, R. Fazio, and M. Collura, Measurement-induced transitions beyond gaussianity: A single particle description, *Phys. Rev. Res.* **6**, 023176 (2024).
- [60] B. Xing, X. Turkeshi, M. Schirò, R. Fazio, and D. Poletti, Interactions and integrability in weakly monitored hamiltonian systems, *Phys. Rev. B* **109**, L060302 (2024).
- [61] M. Szyniszewski, A. Romito, and H. Schomerus, Entanglement transition from variable-strength weak measurements, *Phys. Rev. B* **100**, 064204 (2019).
- [62] R. Nehra, A. Romito, and D. Meidan, (2024), [arXiv:2404.07918](https://arxiv.org/abs/2404.07918) [[quant-ph](https://arxiv.org/abs/2404.07918)].
- [63] M. J. Gullans and D. A. Huse, Dynamical purification phase transition induced by quantum measurements, *Phys. Rev. X* **10**, 041020 (2020).
- [64] M. J. Gullans and D. A. Huse, Scalable probes of measurement-induced criticality, *Phys. Rev. Lett.* **125**, 070606 (2020).
- [65] S. Choi, Y. Bao, X.-L. Qi, and E. Altman, Quantum error correction in scrambling dynamics and

- measurement-induced phase transition, *Phys. Rev. Lett.* **125**, 030505 (2020).
- [66] Y. Bao, S. Choi, and E. Altman, Theory of the phase transition in random unitary circuits with measurements, *Phys. Rev. B* **101**, 104301 (2020).
- [67] Y.-Q. Chen, S. Liu, and S.-X. Zhang, (2024), [arXiv:2405.05076 \[quant-ph\]](#).
- [68] Y. Li and M. P. A. Fisher, Statistical mechanics of quantum error correcting codes, *Phys. Rev. B* **103**, 104306 (2021).
- [69] F. Barratt, U. Agrawal, A. C. Potter, S. Gopalakrishnan, and R. Vasseur, Transitions in the learnability of global charges from local measurements, *Phys. Rev. Lett.* **129**, 200602 (2022).
- [70] Y. Li, R. Vasseur, M. P. A. Fisher, and A. W. W. Ludwig, (2021), [arXiv:2110.02988 \[cond-mat.stat-mech\]](#).
- [71] M. Ippoliti and V. Khemani, Learnability transitions in monitored quantum dynamics via eavesdropper’s classical shadows, *PRX Quantum* **5**, 020304 (2024).
- [72] C. Noel, P. Niroula, D. Zhu, A. Risinger, L. Egan, D. Biswas, M. Cetina, A. V. Gorshkov, M. J. Gullans, D. A. Huse, and C. Monroe, Measurement-induced quantum phases realized in a trapped-ion quantum computer, *Nat. Phys.* **18**, 760 (2022).
- [73] J. M. Koh, S.-N. Sun, M. Motta, and A. J. Minnich, Measurement-induced entanglement phase transition on a superconducting quantum processor with mid-circuit readout, *Nat. Phys.* **19**, 1314 (2023).
- [74] Google Quantum AI and Collaborators, Measurement-induced entanglement and teleportation on a noisy quantum processor, *Nature* **622**, 481 (2023).
- [75] T. Iadecola, S. Ganeshan, J. H. Pixley, and J. H. Wilson, Measurement and feedback driven entanglement transition in the probabilistic control of chaos, *Phys. Rev. Lett.* **131**, 060403 (2023).
- [76] M. Buchhold, T. Müller, and S. Diehl, (2022), [arXiv:2208.10506 \[cond-mat.dis-nn\]](#).
- [77] V. Ravindranath, Y. Han, Z.-C. Yang, and X. Chen, Entanglement steering in adaptive circuits with feedback, *Phys. Rev. B* **108**, L041103 (2023).
- [78] N. O’Dea, A. Morningstar, S. Gopalakrishnan, and V. Khemani, Entanglement and absorbing-state transitions in interactive quantum dynamics, *Phys. Rev. B* **109**, L020304 (2024).
- [79] L. Piroli, Y. Li, R. Vasseur, and A. Nahum, Triviality of quantum trajectories close to a directed percolation transition, *Phys. Rev. B* **107**, 224303 (2023).
- [80] P. Sierant and X. Turkeshi, Controlling entanglement at absorbing state phase transitions in random circuits, *Phys. Rev. Lett.* **130**, 120402 (2023).
- [81] V. Ravindranath, Z.-C. Yang, and X. Chen, (2023), [arXiv:2306.16595 \[quant-ph\]](#).
- [82] A. A. Allocca, C. LeMaire, T. Iadecola, and J. H. Wilson, (2024), [arXiv:2404.16087 \[quant-ph\]](#).
- [83] C. LeMaire, A. A. Allocca, J. H. Pixley, T. Iadecola, and J. H. Wilson, (2023), [arXiv:2309.04520 \[cond-mat.dis-nn\]](#).
- [84] P. Sierant and X. Turkeshi, Entanglement and absorbing state transitions in (d+1)-dimensional stabilizer circuits, *Acta Phys. Pol. A* **144**, 474–485 (2023).
- [85] Y. Li, Y. Zou, P. Glorioso, E. Altman, and M. P. A. Fisher, Cross entropy benchmark for measurement-induced phase transitions, *Phys. Rev. Lett.* **130**, 220404 (2023).
- [86] Y. Li and M. P. A. Fisher, Decodable hybrid dynamics of open quantum systems with F_2 symmetry, *Phys. Rev. B* **108**, 214302 (2023).
- [87] S. J. Garratt and E. Altman, (2023), [arXiv:2305.20092 \[quant-ph\]](#).
- [88] S. J. Garratt, Z. Weinstein, and E. Altman, Measurements Conspire Nonlocally to Restructure Critical Quantum States, *Phys. Rev. X* **13**, 021026 (2023).
- [89] H. Kamakari, J. Sun, Y. Li, J. J. Thio, T. P. Gujarati, M. P. A. Fisher, M. Motta, and A. J. Minnich, (2024), [arXiv:2403.00938 \[quant-ph\]](#).
- [90] Y. Yanay, B. Swingle, and C. Tahan, (2024), [arXiv:2401.17367 \[quant-ph\]](#).
- [91] G. Passarelli, X. Turkeshi, A. Russomanno, P. Lucignano, M. Schirò, and R. Fazio, Many-body dynamics in monitored atomic gases without postselection barrier, *Phys. Rev. Lett.* **132**, 163401 (2024).
- [92] M. Block, Y. Bao, S. Choi, E. Altman, and N. Y. Yao, Measurement-induced transition in long-range interacting quantum circuits, *Phys. Rev. Lett.* **128**, 010604 (2022).
- [93] S. Sharma, X. Turkeshi, R. Fazio, and M. Dalmonte, Measurement-induced criticality in extended and long-range unitary circuits, *SciPost Phys. Core* **5**, 023 (2022).
- [94] P. Sierant, G. Chiriacò, F. M. Surace, S. Sharma, X. Turkeshi, M. Dalmonte, R. Fazio, and G. Pagano, Dissipative Floquet Dynamics: from Steady State to Measurement Induced Criticality in Trapped-ion Chains, *Quantum* **6**, 638 (2022).
- [95] T. Müller, S. Diehl, and M. Buchhold, Measurement-induced dark state phase transitions in long-ranged fermion systems, *Phys. Rev. Lett.* **128**, 010605 (2022).
- [96] T. Minato, K. Sugimoto, T. Kuwahara, and K. Saito, Fate of measurement-induced phase transition in long-range interactions, *Phys. Rev. Lett.* **128**, 010603 (2022).
- [97] K. Seetharam, A. Lerose, R. Fazio, and J. Marino, Dynamical scaling of correlations generated by short- and long-range dissipation, *Phys. Rev. B* **105**, 184305 (2022).
- [98] F. Bloch, Zur Theorie des Austauschproblems und der Remanenzerscheinung der Ferromagnetika, in *Zur Theorie des Austauschproblems und der Remanenzerscheinung der Ferromagnetika: Probleme des Atomkernbaues*, edited by F. Bloch (Springer, Berlin, Heidelberg, 1932) pp. 295–335.
- [99] T. Holstein and H. Primakoff, Field Dependence of the Intrinsic Domain Magnetization of a Ferromagnet, *Phys. Rev.* **58**, 1098 (1940).
- [100] J. Van Kranendonk and J. H. Van Vleck, Spin Waves, *Rev. Mod. Phys.* **30**, 1 (1958).
- [101] A. Rückriegel, A. Kreisel, and P. Kopietz, Time-dependent spin-wave theory, *Phys. Rev. B* **85**, 054422 (2012).
- [102] A. Lerose, B. Žunkovič, J. Marino, A. Gambassi, and A. Silva, Impact of nonequilibrium fluctuations on prethermal dynamical phase transitions in long-range interacting spin chains, *Phys. Rev. B* **99**, 045128 (2019).
- [103] G. Vidal, J. I. Latorre, E. Rico, and A. Kitaev, Entanglement in Quantum Critical Phenomena, *Physical Review Letters* **90**, 227902 (2003).
- [104] N. Gisin and I. C. Percival, The quantum-state diffusion model applied to open systems, *J. Phys. A: Math. Theor.* **25**, 5677 (1992).
- [105] M. Kac, G. E. Uhlenbeck, and P. C. Hemmer, On the

- van der Waals Theory of the Vapor-Liquid Equilibrium. I. Discussion of a One-Dimensional Model, *J. Math. Phys.* **4**, 216 (1963).
- [106] G. Ferioli, A. Glicenstein, F. Robicheaux, R. T. Sutherland, A. Browaeys, and I. Ferrier-Barbut, Laser-Driven Superradiant Ensembles of Two-Level Atoms near Dicke Regime, *Phys. Rev. Lett.* **127**, 243602 (2021).
- [107] W. Verstraelen, D. Huybrechts, T. Roscilde, and M. Wouters, Quantum and Classical Correlations in Open Quantum Spin Lattices via Truncated-Cumulant Trajectories, *PRX Quantum* **4**, 030304 (2023).
- [108] W. Verstraelen and M. Wouters, Gaussian quantum trajectories for the variational simulation of open quantum-optical systems, *App. Sci.* **8**, 1427 (2018).
- [109] W. Verstraelen, R. Rota, V. Savona, and M. Wouters, Gaussian trajectory approach to dissipative phase transitions: The case of quadratically driven photonic lattices, *Phys. Rev. Res.* **2**, 022037 (2020).
- [110] P. E. Kloeden, E. Platen, P. E. Kloeden, and E. Platen, *Stochastic differential equations* (Springer, 1992).
- [111] A. Serafini, F. Illuminati, and S. D. Siena, Symplectic invariants, entropic measures and correlations of Gaussian states, *J. Phys. B* **37**, L21 (2003).
- [112] Note that it can be computationally more practical to diagonalize the dissipator first (see Appendix A) and work in the basis where the noise becomes diagonal, in which case the covariance matrix \mathbf{K} also diagonalizes and it suffices to generate independent Gaussian random numbers to approximate the noise.
- [113] The entanglement entropy is calculated following the derivation in [7]. One can also choose any other nonlinear function of the state for this benchmark.
- [114] F. Iemini, A. Russomanno, J. Keeling, M. Schirò, M. Dalmonte, and R. Fazio, Boundary time crystals, *Phys. Rev. Lett.* **121**, 035301 (2018).
- [115] G. Piccitto, M. Wouters, F. Nori, and N. Shammah, Symmetries and conserved quantities of boundary time crystals in generalized spin models, *Phys. Rev. B* **104**, 014307 (2021).
- [116] A. Cabot, L. S. Muhle, F. Carollo, and I. Lesanovsky, Quantum trajectories of dissipative time crystals, *Phys. Rev. A* **108**, L041303 (2023).
- [117] J. Preskill, Quantum Computing in the NISQ era and beyond, *Quantum* **2**, 79 (2018).
- [118] T. A. Brun, A simple model of quantum trajectories, *American Journal of Physics* **70**, 719–737 (2002).
- [119] J. A. Gross, C. M. Caves, G. J. Milburn, and J. Combes, Qubit models of weak continuous measurements: markovian conditional and open-system dynamics, *Quantum Science and Technology* **3**, 024005 (2018).
- [120] Note that since the random variable $\Delta R_x \Delta R_y$ has negligible variance (of the order Δt^2), we replace it with the mean: $\Delta R_x \Delta R_y = \overline{\Delta R_x \Delta R_y} = 0$ [123]. Therefore, terms proportional to $\Delta R_x \Delta R_y$ are dropped in this derivation.
- [121] P. M. Poggi and M. H. Muñoz-Arias, Measurement-induced multipartite-entanglement regimes in collective spin systems, *Quantum* **8**, 1229 (2024).
- [122] H.-P. Breuer and F. Petruccione, *The theory of open quantum systems* (OUP Oxford, 2002).
- [123] I. Percival, *Quantum state diffusion* (Cambridge University Press, 1998).